REVISION 2

Secondary minerals associated with Lassen fumaroles and hot springs: implications for Martian hydrothermal deposits

Lindsay J. McHenry[1•]
George L. Carson[1]
Darian T. Dixon[1,2]
Christopher L. Vickery[1]

[1] Department of Geosciences, University of Wisconsin-Milwaukee, 3209 N. Maryland Ave., Milwaukee, WI 53211, U.S.A.

[2] Present address: Geology Department, Western Washington University, 516 High St, Bellingham, WA 98225.

• Corresponding author: lmchenry@uwm.edu. 1 414 229-3951

For submission to American Mineralogist

Abstract

The active hot springs, fumaroles, and mud pots of the southwestern Lassen hydrothermal system include a variety of alteration environments, which produce a range of

hydrothermal mineral assemblages. Analysis of water, mineral precipitates, altered sediment, and rock samples collected at and near these features at Sulphur Works, Bumpass Hell, Little Hot Springs Valley, and Growler and Morgan Hot Springs reveals conditions ranging from ~100° C acid-sulfate fumaroles (e.g. Sulphur Works and Bumpass Hell) to near-neutral hot springs (e.g. Growler and Morgan), and includes both oxidizing and reducing conditions. Resulting hydrothermal minerals include a wide variety of sulfates (dominated by Al-sulfates, but also including Fe^{2+}, Fe^{3+}, Ca, Mg, and mixed-cation sulfates), sulfides (pyrite and marcasite), elemental sulfur, and smectite and kaolinite clays. Most altered samples contain at least one silica phase, most commonly quartz, but also including cristobalite, tridymite, and/or amorphous silica. Quartz and other silica phases are not as abundant in the less altered rock samples, thus their abundance in some hydrothermally altered sediment samples suggests a detrital origin, or formation by hydrothermal alteration (either modern or Pleistocene); this requires a high degree of diagenetic (or epigenetic) maturation. These results support a previously identified model that the Lassen hydrothermal system involves the de-coupling of a vapor phase (which becomes acidic as it oxidizes near the surface, producing acid-sulfate fumaroles at higher elevations at Sulphur Works and Bumpass Hell) from the residual near neutral thermal waters that emerge as hot springs at lower elevations (Growler and Morgan). Because both acid-sulfate fumarole and near-neutral sinter-producing hot springs have been invoked to explain the silica-rich deposits observed by the Mars Exploration Rover Spirit near Home Plate in the Columbia Hills on Mars, Lassen can serve as a useful terrestrial analog for comparison.

47 **Keywords: Mars, hydrothermal alteration, sulfate minerals, element mobility**

Introduction and Background

The Lassen Hydrothermal System

The Lassen hydrothermal system in Northern California is the largest active hydrothermal field in the Cascades, with widespread fumaroles, hot springs, and mud pots (e.g. Ingebritsen et al., 2016). These fluids and gases represent varied temperature, pH, and oxidation conditions, and interact with the dacitic to andesitic host rocks, producing a range of alteration minerals related to variable hydrothermal conditions.

Cascade volcanic activity in the Lassen area began ~3.5 Ma ago, with both short-lived calc-alkaline volcanism and longer-term volcanism associated with a series of five volcanic centers, which included both silicic and andesitic products. These longer-lived volcanic centers (Yana, Maidu, Dittmar, Latour, and the still active Lassen) developed hydrothermal systems at various stages during their histories (e.g. John et al., 2005, 2009) but often late, as circulating groundwater was heated by cooling silicic magma at depth (Muffler and Clynne, 2015). Volcanism associated with the Lassen Volcanic Center started about 825,000 years ago with the Rockland caldera complex (825,000 – 611,000 yrs) followed by the Brokeoff Volcano (550,000 – 350,000 yrs), and finally the Lassen dome field (~315,000 – 0 yrs). In addition to the currently active Lassen hydrothermal system, two relict hydrothermal systems have been identified associated with Brokeoff Volcano. Current active hydrothermal activity is in places superimposed upon the eroded and exposed remnants of these older hydrothermal systems, which can complicate efforts to isolate the effects of the modern hydrothermal system.

Currently, acid sulfate fumarole and/or hot water discharge areas include Bumpass Hell, Sulphur Works, the Pilot Pinnacle area, and Little Hot Springs Valley in the southwestern part of the park (with Growler and Morgan Hot Springs several kilometers south beyond the park boundaries), along with Devil's Kitchen, Boiling Springs Lake, Drakesbad Hot Spring, and Terminal Geyser to the southeast (Figure 1). Most are steam-heated acid-sulfate systems, though Drakesbad, Growler, and Morgan Hot Springs discharge more neutral, chlorine-rich hydrothermal fluids and lower Sulphur Works and upper Little Hot Springs Valley have some bicarbonate-dominated springs in addition to their acid-sulfate fumaroles and hot springs (Muffler et al., 1982; Thompson et al., 1985; Clynne et al., 2003). Most of the hydrothermal waters are isotopically consistent with exchanged local meteoric waters suggesting a local source, though some signatures of mantle-derived volatiles (CO_2, H_2S, N_2) are observed at Sulphur Works (Janik and McLaren, 2010). The current study focuses on the southwestern hydrothermal system.

Prior studies of the Lassen hydrothermal system support a model that links the steam-driven acid-sulfate areas (e.g. Bumpass Hell) and the near-neutral, Cl-rich hot springs (e.g., Morgan and Growler). Muffler et al. (1982), Janik and McLaren (2010), and Ingebritsen et al. (2016) propose a model in which the same heated reservoir of meteoric water is separated at depth by boiling, which partitions the sulfur (as H_2S), CO_2, and other trace gases into the vapor phase that rises towards the surface. The H_2S is oxidized forming H_2SO_4 as it approaches the surface, and emerges as acid sulfate fumaroles and springs at higher elevations. Boiling leaves behind hot, neutral pH water enriched in Cl that emerges as hot springs at lower elevations (Figure 2). This separation occurs due to

differences in solubility of different constituents in thermal water; Cl^- is more soluble in the liquid phase (hot water), whereas CO_2, H_2S, and other trace gases are strongly partitioned into the vapor phase (steam) (e.g. White et al., 1971). In this model (as applied to the Lassen hydrothermal system), both silica sinter deposits and acid-leached fumarolic residues form from the same system, albeit in much different locations. Little Hot Springs Valley is more complex, with near-neutral pH travertine-depositing hot springs near its headwaters and a combination of acid-sulfate fumaroles and both acidic and near-neutral hot springs further down the drainage.

These active hydrothermal centers have altered the surrounding and underlying rock, which for Sulphur Works and Little Hot Springs Valley consists largely of landslide blocks derived from rocks upslope. These blocks are predominantly andesite and in some cases previously hydrothermally altered, either from recent interaction with the modern hydrothermal system (hydrothermal activity extends about 1 km north (upslope) of Sulphur Works) or by previous episodes of hydrothermal alteration associated with Brokeoff Volcano. This older alteration can include pyrite, alunite, kaolinite, pyrophyllite, dickite, and a range of silica phases including quartz (John et al., 2006). Bumpass Hell host rocks include both dacite and andesite (Clynne et al., 2008). Less altered host rocks are also present at a distance (typically tens of meters) from the hydrothermally altered areas, thereby allowing comparison between fresh and altered rock compositions to help reconstruct the patterns and processes of alteration. These patterns, however, could result from multiple episodes of alteration and might not be related exclusively to the active hydrothermal system.

117

118 **Hydrothermal deposits in the Columbia Hills, Mars**

119 Hydrothermal environments were likely common on Mars (due to evidence of early
120 aqueous activity (e.g. Hynek et al., 2010) and a long record of volcanic activity (e.g.
121 Phillips et al., 2001; Bibring et al., 2006; Robbins et al., 2011), and such environments
122 could have remained habitable long after the surface cooled and desiccated (e.g. Walter
123 & Des Marais, 1993; Schulze-Markuch et al., 2007). However, some hydrothermal
124 environments are more habitable than others, and being able to distinguish between the
125 deposits of hostile acid-sulfate fumarole and more accommodating near-neutral hot
126 spring environments can provide clues to habitability. On Earth life exists in both
127 environments, but the biomass and microbial diversity of near-neutral hot springs can be
128 orders of magnitude higher than that of acid-sulfate fumaroles, while the biota of
129 fumaroles tends to be limited to highly specialized thermophilic extremophiles (e.g.
130 Goorissen et al., 2003; Krebs et al., 2014) which may have evolved from organisms
131 suited to more neutral environments (Yen et al., 2008). Very acidic conditions could pose
132 significant limitations on models for the origin of life (Knoll et al., 2005). Additionally,
133 silica sinters readily encrust biological remains and preserve biologically-mediated
134 textures, preserving a record of past life (e.g. Konhauser et al., 2001; Geptner et al., 2005;
135 Ruff et al., 2016).

136

137 Opal-A and sulfate-rich deposits in outcrops and soils in Gusev crater's Columbia Hills,
138 investigated in situ by the Mars Exploration Rover (MER) Spirit, are interpreted to have
139 formed under a range of hydrothermal conditions. Proposed hydrothermal environments

include acid-sulfate fumaroles (e.g. Squyres et al., 2007, 2008; Schmidt et al., 2009), warm acid-sulfate hot springs (Squyres et al., 2008), or near-neutral Cl-rich hot springs (Ruff et al., 2011). Evidence supporting a hydrothermal origin for these deposits includes elevated silica contents (likely a result of sinter precipitation or acid leaching), Ti contents (more consistent with acid leaching), and elevated S, Cl, and Br concentrations often associated with hydrothermal fluids (Squyres et al., 2008; Schmidt et al., 2008; Yen et al., 2008). The presence of Fe-sulfate minerals and the relative abundance of Cl and S (consistent with partitioning between a liquid and vapor phase) suggest acid-sulfate hydrothermal fluids (Squyres et al., 2007, 2008), potentially fumaroles (Squyres et al., 2007; Schmidt et al., 2009), though the depletion of less volatile elements in the altered rock may have required liquids for transport (Squyres et al., 2008). The apparent transport of non-volatile elements (e.g. Al, Na, Fe) in the altered deposits suggests a high water:rock ratio in the Si-rich soils (e.g. Eastern valley soils: Morris et al., 2008, Squyres et al., 2008), but apparently isochemical alteration of other rocks (e.g. Watchtower class, where bulk compositions remain basaltic despite the formation of secondary minerals including goethite, palagonite, and hematite: Morris et al., 2008) suggests lower water-rock ratios (Wang et al., 2008), consistent with vapor phase (potentially fumarolic) alteration.

Ruff et al. (2011) argue that the silica-rich deposits adjacent to Home Plate in the Columbia Hills are not consistent with leaching by acid-sulfate fumaroles, but rather resulted from precipitation of a silica-rich sinter (dominated by Opal-A) from near-neutral fluids. Ruff et al. (2011) and Ruff and Farmer (2016) also use morphology,

163 textures, and stratigraphic position to support a silica-rich sinter origin; the nodular
164 texture associated with high-Si "outcrops" (e.g. Elizabeth Mahon) examined by Spirit
165 more closely resembles terrestrial sinters than acid-sulfate-related residues. Because there
166 are also acid-sulfate related hydrothermal minerals in the vicinity, this would necessitate
167 a diverse set of hydrothermal conditions, either from multiple episodes of hydrothermal
168 activity with different characteristics, or a single, varied hydrothermal system. The
169 interpretation of these deposits depends on our ability to distinguish between the products
170 of alteration under varied hydrothermal conditions, which can be addressed in part by
171 studying analog environments on Earth.
172
173 **Lassen as a Mars analog**
174 The Lassen hydrothermal system provides a wide range of hydrothermal environments,
175 including fumaroles, acid-sulfate hot springs and mud pots, and near-neutral, Cl-rich hot
176 springs. This provides an opportunity to assess the diversity of alteration products
177 produced under varied conditions by a single hydrothermal system as it interacts with
178 volcanic rocks, thereby providing a useful comparison to the hydrothermal deposits in
179 the Columbia Hills on Mars.
180
181 **Objectives**
182 The objectives of this work are to (1) document the hydrothermal phases present at and
183 near Lassen fumaroles and hot springs, (2) relate these phases to temperature, pH,
184 oxidation state, and other intensive variables of Lassen hydrothermal fluids, (3) assess
185 element mobility (leaching, enrichment) during hydrothermal alteration at Lassen, and (4)

compare these deposits to proposed hydrothermal deposits in the Columbia Hills of Gusev crater, Mars.

Methods

Field methods

Fumarole and hot spring sampling was conducted in September-October of 2012, 2013, 2014, and 2016. Samples were collected at Sulphur Works, Bumpass Hell, Little Hot Springs Valley, and Growler and Morgan Hot Springs. Samples were selected based on color, texture, and context to cover the entire range of alteration and precipitate deposits observed. Soft precipitates and altered soils were scooped into sample bags; host rocks and coatings on harder rocks were collected using a rock hammer. The appearance and position relative to the nearest thermal feature were described for each sample, along with temperature at the sample site (for samples collected in 2013 and 2014). For samples collected adjacent to liquid water, the temperature and pH of the water were also measured using a thermometer and either pH paper or a Hydrolab Sonde. In 2014, four narrow "pits" were excavated in Little Hot Springs Valley using a hand trowel, to assess variation with depth. All solid samples and their locations are briefly described in Table 1; for samples collected in contact with or directly adjacent to liquid water (as indicated in the sample description), the pH of that water is also listed associated with the solid sample. Figure 3 shows examples of sampling sites, with samples indicated. Samples from the four Little Hot Springs Valley pits are attributed to Pits 1-4, with sample depth indicated.

Water samples were also collected or analyzed in situ using a Hydrolab Sonde (in 2013 and 2014). For standing or flowing water under 50° C, the Hydrolab Sonde was inserted directly into the water for in-situ analysis. For water over 50° C, water was collected in a jar that had been rinsed several times with the water to be sampled (pre-contaminated) and allowed to cool (sealed, and full to minimize interaction with the atmosphere) to below 50° C, at which time the Hydrolab Sonde was inserted into the jar for analysis. The Hydrolab data includes pH (accuracy ± 0.2 pH units), temperature (T, at time of analysis, ± 0.1 °C), specific conductivity (SpCond, ± 0.5% of reading + 0.001 mS/cm), resistivity (Res, kΩ/cm), oxidation/reduction potential (ORP, ± 20 mV), salinity (Sal, ± 0.2 parts per thousand), and total dissolved solids (TDS, g/L) (Table 2). The pH sensor on the Hydrolab Sonde failed during the 2014 expedition, thus some pH values reported from that year are approximated from pH papers of overlapping ranges.

Laboratory methods

Sample preparation and data interpretation for X-ray Diffraction (XRD). Samples were air dried in the lab in aluminum trays for several days. Soft precipitate samples and altered soil samples were then hand-ground in an agate mortar and pestle without liquid or heat, to prevent the alteration of temperature-sensitive or soluble minerals. Thin, hard coatings were removed and powdered using a dental drill, and rock samples were powdered using a tungsten carbide shatterbox. Samples were mounted as random powders for X-Ray Diffraction (XRD) and analyzed using a Bruker D8 Focus XRD (Cu tube, 0.02° 2θ step size, 2 – 60° 2θ, 1 second/step) following the methods described in McHenry (2009). Mineral phases were identified using Bruker's EVA software, using the

International Centre for Diffraction Data Powder Diffraction Files (ICDD PDF) 2 database for comparison. This software matches the diffraction pattern measured by the instrument (peak positions and relative peak heights) against the patterns derived from mineral phases for which structural information is available in the database, suggesting likely matches which can be assessed by the user. Qualitative relative abundances were estimated using relative peak heights, and are reported in Tables 3 and 4 as abundant, common, between common and rare, rare, or absent.

Sample preparation and data interpretation for X-ray Fluorescence. Most alteration, sediment, and substrate samples were also prepared for X-ray Fluorescence (XRF) analysis. Samples were dried overnight at 105°C, then 1 +/-0.003 grams of powdered sample were combined with 10 +/-0.003 grams of a 50:50 lithium metaborate/ tetraborate flux (with integrated LiBr non-wetting agent) and ~1 gram of ammonium nitrate (oxidizer) and fused for ~20 minutes using a Claisse M4 fluxer. Loss on Ignition (LOI) was determined by heating ~0.5 grams of each sample (precisely weighed) in a pre-ignited ceramic crucible in a muffle furnace at 1050°C for 15 minutes. Where limited material was available, the powdered sample discarded following XRD analysis was used for LOI. Fused beads were then analyzed for major and minor elements using a Bruker S4 Pioneer Wavelength Dispersive (WD) XRF. Data were calibrated using a calibration curve derived from 11 USGS rock standards. More detailed methods, including method-related error estimates, can be found in McHenry (2009), updated in Byers et al. (2016).

The fused bead analyses do not include sulfur (it is partially lost under the fusion conditions used), thus pressed pellets were also analyzed for representative samples for which sufficient material was available. Then, 7.5 grams of dried sample was combined with three Bruker GeoQuant wax binder pellets (0.94 g total) using a shatterbox for 30 seconds. This powder was then pressed in a 40 mm die using an Atlas T25 press at 25 tons for 1 minute. More details on the methods employed are provided in Byers et al. (2016). These pressed pellets were then analyzed using the Bruker S4 Pioneer, and calibrated using a calibration curve derived from 6 USGS rock standards. Because the precision and reproducibility of the analyses are better for the fused beads (see McHenry et al., 2011), only the sulfur value from the pressed pellet analysis is provided, with the remaining elements reported from the fused bead analysis of the same sample. Note that the reported totals include the elements (as oxides) determined from the fused beads and the LOI value (and not the SO_3 concentration), because SO_3 is partially lost during the fusion (and LOI) process.

Sample preparation for microscopy (petrographic and SEM)

Select samples of coated rocks, rock coatings, and altered rocks were sent out for petrographic thin sectioning (polished surface). Thin sections were first examined and photographed using a petrographic microscope to identify minerals and determine textures. Four thin sections were then carbon coated and analyzed using a Hitachi S-4800 Field Emission Scanning Electron Microscope (FE-SEM) equipped with a Bruker Quantax Energy Dispersive Spectroscopy (EDS) system. Secondary electron and Backscattered electron (SE and BSE) imaging provided textural and general

277 compositional information, while EDS provided qualitative elemental abundances to aid
278 in mineral identification.
279
280 **Results**
281 **Water samples**
282 Surface waters associated with the Lassen hydrothermal system vary in temperature, pH,
283 and other parameters, as measured using pH paper, a thermometer, and/or the Hydrolab
284 sonde (see Table 2). Sulphur Works bubbling hot springs were acidic (pH 2.07-2.33) and
285 hot (T 68°-84°C), and varied from oxidizing to slightly reducing (both positive and
286 negative ORP values). Bumpass Hell hot springs were acidic (pH 2.02-2.39), warm to hot
287 (T 27.1°-88.6°C), and for the most part, reducing. Little Hot Springs Valley showed more
288 varied conditions, with both near-neutral hot springs (pH 6.4-6.6, T 65.7-91.0°C) and
289 acidic hot springs (pH 1.70-2.20; T 75.0-82.0°C), though all waters were reducing.
290 Growler and Morgan Hot Springs, to the south of Lassen Volcanic National Park, were
291 near-neutral (pH 7.0-8.1), warm to hot (T 49.6-93.5°C), reducing, and more saline
292 (salinity 5.3-6.2 parts per thousand).
293
294 **XRD results**
295 Phases identified in the XRD patterns include a wide range of secondary minerals, listed
296 in Tables 3 (non-sulfates) and 4 (sulfates). Most of the sediment and altered rock samples
297 also contain some primary igneous minerals, mainly augite and plagioclase (classified in
298 Table 3 as “substrate”). Few sample contain minor K-feldspar, possibly adularia. Silica
299 phases, including quartz, tridymite, cristobalite, and amorphous silica, are also

widespread and abundant in the altered materials. The sulfate minerals are dominated by Al-rich phases (principally alunogen and alunite) and Fe-rich phases (including jarosite), but also include mixed cation varieties and gypsum. Clay minerals (smectite and/or kaolinite) are also abundant and widespread. Other phases of note include hematite, goethite, pyrite, marcasite, calcite, and halite. Figure 4 shows representative XRD plots for a variety of sample types.

Silica phases. Quartz is one of the most abundant minerals in most altered samples from Sulphur Works (e.g. L-SW-12-14, Figure 4A), whereas a few samples have amorphous silica or cristobalite and/or tridymite in addition to or instead of quartz. These silica phases (along with microquartz and chalcedony) can be distinguished using their XRD patterns, though less crystalline varieties (e.g. opal-A, opal-C, silicic glasses) show "humps" with few, broad, or no peaks (Graetsch, 1994). At Sulphur Works, only the host rock sample and the three samples of pure alunogen crystal precipitates from the very surface do not contain a silica phase. The lack of quartz in the andesitic Sulphur Works rock sample and its absence or near absence in the three additional less-altered host rock samples collected in 2016 indicates that this phase must be secondary in the altered samples and not a primary igneous mineral, though it might have been derived from previously altered materials resulting from Pleistocene hydrothermal systems (John et al., 2006). At Bumpass Hell quartz is less common; although all samples contain at least one silica phase, it can be quartz, cristobalite, tridymite, amorphous silica, or a combination of these (e.g. L-12-BH-3). Quartz is less abundant or absent in the samples with abundant sulfide minerals. Samples from Little Hot Springs Valley did not contain tridymite or

cristobalite and only rarely contain amorphous silica, but most samples contained abundant quartz except for calcite-dominated travertines associated with near-neutral bicarbonate hot springs near the headwaters (samples L-LV-14-25, 27, and 29). Near Growler and Morgan Hot Springs, amorphous silica dominates (e.g. L-13-G-2, Figure 4D), with quartz and cristobalite observed in only one sample (from a nearby fumarole, which also contained alunite, jarosite, and other sulfate phases typically associated with acidic fluids).

Sulfates, sulfides, and native sulfur. Sulfate minerals were observed in all areas of the hydrothermal system, and covered a range of compositions. Al-sulfates were most common (and diverse), though Fe-sulfates were also abundant in some samples. Gypsum was rare, found only in a few samples from Little Hot Springs Valley and Growler and Morgan Hot Springs, often associated with more neutral fluids (e.g. L-13-G-2, Figure 4D). Mg-sulfates were not observed, except for possible pickeringite in a few samples from Little Hot Springs Valley (e.g. L-LV-14-16, Figure 4C).

Sulfides (pyrite and marcasite) were identified in few samples from Bumpass Hell (e.g. L-12-BH-5, Figure 4B) and Little Hot Springs Valley (associated with more reducing water conditions, indicated by a negative ORP), and absent from samples collected at other sites in this study. Elemental sulfur was observed in some samples collected directly adjacent to fumarole vents at Sulphur Works, Bumpass Hell, and Little Hot Springs Valley.

346 **XRF results**

347 The XRF data for all precipitate, sediment, rock, and substrate samples analyzed are
348 reported in Tables 5 (major elements) and 6 (trace elements). The compositions of the
349 less altered rock samples from Sulphur Works (andesite), Bumpass Hell (weakly altered
350 dacite), and Little Hot Springs Valley (andesite) provide a starting point for determining
351 patterns of element mobility during alteration. Analyses of the three less altered rock
352 samples were plotted on the Le Bas et al. (1986) total alkali-silica diagram to determine
353 rock type; this determination agrees with prior characterization of volcanic rocks from
354 these sites (e.g. Clynne et al., 2008). The substrate sample for Bumpass Hell (L-12-BH-8)
355 was weakly altered, therefore we used an analysis of the Bumpass dacite from Clynne et
356 al. (2008) for comparison. Altered rock and sediment samples from Sulphur Works (acid-
357 sulfate fumarole environment) tend to be elevated in SiO_2 and depleted in Na_2O, MgO,
358 K_2O, and CaO relative to the less altered andesitic substrate (Figures 5 and 6). TiO_2 and
359 Zr are residually enriched in most but not all altered rock and sediment samples. The
360 concentrations of Fe (all Fe reported as Fe_2O_3) and Al_2O_3 can be enriched, depleted, or
361 preserved depending on which authigenic phases dominate the assemblage.
362
363 **Petrographic and SEM results**
364 A textural analysis of samples using thin sections illustrates the biogenic nature of some
365 precipitated silica coatings, especially at Growler Hot Spring (Figures 7 and 8). EDS
366 analysis confirms that the thicker coatings (L-13-G-2 and 3) are mostly silica, with minor
367 inclusions of other minerals (a Cl-bearing phase, a Mg-Ca phase, most likely dolomite,
368 and likely detrital grains of pyroxene). A coating in a sample from Little Hot Springs

Valley (L-LV-14-14) contains layers of both silica and gypsum. L-BH-12-2 represents an altered rim of a dacitic block, in which minerals on the outside are more degraded than those on the interior. Silica phases occur within the groundmass; according to the XRD results, quartz, tridymite, and cristobalite are all present in this altered rim (the interior was not analyzed by XRD for comparison).

Discussion

Relationship between alteration minerals and hydrothermal conditions

The mineral associations identified can be related to the environmental conditions observed. For example, the more oxidizing conditions observed associated with the acid-sulfate fumaroles at Sulphur Works produce sulfates and native sulfur but fewer sulfide minerals, and Fe-bearing alteration phases are dominated by those with Fe^{3+} (e.g. jarosite). In contrast, the more reducing Bumpass Hell fumaroles and hot springs produce a wider range of alteration products, including abundant sulfides (pyrite and marcasite), but less abundant sulfates (though the observed Fe-bearing sulfates are Fe^{3+} phases). The sulfides were most abundant in fine-grained dark "foams" floating in hot springs and are clearly authigenic precipitates rather than residues from previous hydrothermal episodes. Near-neutral, more saline fluids at Growler Hot Spring are associated with amorphous silica sinter precipitates, with minor gypsum and halite (Figure 4D), two phases that are absent at the sites with more acidic, less saline fluids (e.g. Sulphur Works and Bumpass Hell). Except for gypsum, sulfate minerals observed in this study show an association with acidic conditions. In this study calcite was observed exclusively in travertines associated with the near-neutral thermal waters of upper Little Hot Spring Valley.

392

393 **Ephemeral phases- annual variation at Sulphur Works**

394 Many of the sulfate minerals observed in the Lassen hydrothermal areas are water soluble
395 and not stable for long time periods under the temperate but wet conditions at Lassen. We
396 collected samples from the same fumarole at Sulphur Works (pictured in Figures 2A and
397 9) during each of our three sampling visits and noted significant changes in the
398 appearance and extent of the precipitated alunogen crystals. In 2012 (sample L-SW-12-4)
399 these precipitates included bundles of fibrous alunogen several cm in length, while in
400 2013 (L-13-SW-1) and 2014 (L-SW-14-03) the same deposit consisted of much smaller
401 crystals and had a much more powdery appearance. XRD analyses revealed only
402 alunogen in 2012 and 2013 samples, and alunogen plus halotrichite and/or pickeringite in
403 2014 samples. While no copiapite was observed in this study, it is possible that this
404 highly unstable Fe-bearing sulfate mineral (e.g. Bigham and Nordstrom, 2000) was
405 initially present, but degraded rapidly as the deposit dried or even after sampling prior to
406 XRD analysis. We noted that the fumarole was less active (emitting less steam) in 2014
407 than in the prior two years, perhaps due to locally drier conditions at the same time of
408 year. These soluble precipitated phases are sensitive to the vigor of the associated
409 fumarole (which was visibly less active in 2014 than in 2012), and to local surface water
410 availability. Day and Allen (1925) first noted seasonal and annual variations in the vigor
411 of Lassen hydrothermal activity.

412

413 **Quartz vs. amorphous silica**

414 The presence of crystalline silica phases (quartz, cristobalite, and/or tridymite) in addition
415 to (or instead of) amorphous silica reflects the dacitic to andesitic compositions of the
416 host rock, and could also reveal a significant level of mineralogical maturation. Quartz
417 can be present in dacitic to andesitic substrate material (and has been previously
418 documented in Bumpass Hell dacites), and cristobalite and tridymite can both be formed
419 as high-temperature vapor phases filling vesicles and groundmass microcavities in silicic
420 volcanic rocks (e.g. Pallister et al., 2008). The quartz, tridymite, and cristobalite-rich
421 samples in our study often lacked other primary igneous phases (feldspars and pyroxene),
422 suggesting a secondary or detrital origin for these silica phases, though in altered rock
423 sample L-BH-12-2 a crystalline silica phase is identified in the groundmass associated
424 with plagioclase and pyroxene phenocrysts (Figures 7 and 8). Additionally, the XRD
425 patterns for the less altered rock samples (all of which contained plagioclase and
426 pyroxene minerals) lacked or nearly lacked silica phases. Another possibility is that these
427 silica phases derived from previously altered rocks from the Pleistocene hydrothermal
428 systems, in which quartz is common (e.g. John et al., 2006).
429
430 One instance in which quartz appears to have originated within the modern hydrothermal
431 environment (rather than from Pleistocene hydrothermal alteration, or through igneous
432 processes) is sample L-LV-14-14. This sample comes from a rock that appeared to have
433 acquired its silica-rich coating in the local environment, as it was found in a stream
434 among many other similar rocks with white coatings on the surfaces facing upwards into
435 the stream (as if they were coated in situ, rather than having been previously coated and
436 transported to this site). The only silica phase identified in the XRD results for this

437 coating is quartz (no amorphous "hump" was observed). SEM analysis (Figure 8) reveals
438 a silica-rich coating with intervals of gypsum, which was also recognized using XRD.
439
440 Previous studies have found that quartz takes ~10,000 years to form from opal-A
441 originally formed in silica sinter environments (e.g. Herdianita et al., 2000), an
442 unreasonably long time frame for currently active fumaroles and hot springs at Lassen.
443 Rodgers et al. (2002, 2004) found that opal-A (formed initially as a silica residue of acid-
444 sulfate fumarolic alteration of volcanics) matured to quartz within several thousand to
445 several tens of thousands of years in the Taupo and other volcanic zones of New Zealand,
446 assisted in part by elevated temperatures. However, Lynne et al. (2007) found that in
447 sinter hot spring environments in the Taupo Volcanic Zone, quartz can develop from
448 opal-A on much shorter time scales (centuries, rather than millennia), more consistent
449 with the likely time frame associated with the silicic deposits observed at Lassen. Lynne
450 et al. (2006) further found that opal-A in silica sinters later exposed to fumarolic
451 conditions can begin the transformation to chalcedonic quartz within months. In all these
452 studies, quartz (or chalcedonic quartz) forms from opal-A in a series of steps involving
453 opal-C and opal-CT (e.g. Rodgers et al., 2004), and none involved tridymite or
454 cristobalite (which typically form stably only at higher temperatures, though both have
455 been observed in trace amounts in modern Icelandic sinter: Preston et al., 2008).
456
457 At Lassen, silica phases formed by older hydrothermal systems that affected Brokeoff
458 Volcano and which have had much longer times (100,000s of years) to recrystallize could
459 confuse this interpretation, especially for Sulphur Works and upper Little Hot Springs

Valley where landslide-deposited blocks of this previously altered material make up part of the host rock.

Oxidizing vs. reducing environments

The variety of hydrothermal minerals observed is closely tied to variable conditions of alteration. At Sulphur Works, where hydrothermal fluids are more oxidizing, sulfur-bearing phases are limited to elemental sulfur (near the center of active fumaroles) and sulfate minerals, at least at and near the surface at fumaroles. At Bumpass Hell, where more reduced waters are also present, sulfur-bearing phases include abundant sulfide minerals. Most sulfide-bearing samples also contained minor sulfates (alunite, alunogen, and/or rhomboclase). While some of these sulfide- and sulfate-bearing assemblages could be tied to older episodes of hydrothermal activity, the fine-grained dark sulfide "foam" floating in reducing hot springs also contains some sulfate minerals, likely resulting from oxidation of newly precipitated sulfides in the modern hydrothermal environment. Additionally, the presence of fine-grained sulfide minerals at depth (10s of cm; e.g. L-LV-14-23 in Little Hot Springs Valley, Figure 3D) but not at the surface in currently active hydrothermal areas with reducing fluid conditions suggests the precipitation of these phases in the modern environment. Interaction with oxygenated surface water (or the atmosphere) leads to a shallow oxidation front, with fine-grained sulfides present below. The near-neutral and slightly more saline conditions present at Growler Hot Spring resulted in the precipitation of halite along with amorphous silica sinter and minor gypsum.

The species of *Archaea*, bacteria, and algae in the Lassen hydrothermal area play a significant role in the origin of the acid-sulfate systems (e.g. Siering et al., 2006). The redox conditions of the Lassen hydrothermal system are in part due to the actions of sulfur and iron reducing and oxidizing bacteria, which affects the redox state of the fluids even before they reach the surface and are exposed directly to the atmosphere (Siering et al., 2006; Arroyo et al., 2015).

Element mobility during hydrothermal alteration

Most major elements show evidence for leaching, when fumarole-altered samples are compared to less altered rocks (Figures 5, 6, and 10). MgO, CaO, Na_2O, and K_2O are universally depleted, whereas Fe_2O_3 and Al_2O_3 can be either depleted or enriched depending on the secondary mineral assemblage. SiO_2 is enriched in most samples. These trends are consistent with open-system acid-sulfate leaching, which removes the more mobile cations from the system, residually enriching silica (and in some cases titanium). Samples that retain their Al_2O_3 appear to be either the least altered samples (for example, sediments that retain original substrate mineral assemblages, including augite and plagioclase) or samples with significant clay components.

Figures 5 and 6 show alteration trends in the form of spider diagrams for the major elements for the altered samples, normalized to the Zr concentration of a local less altered rock sample for three areas (Sulphur Works, Bumpass Hell, and Little Hot Springs Valley). Zr was chosen for normalization because it showed the least variation between samples at Sulphur Works and is typically conserved during weathering and

hydrothermal alteration (e.g. Summa and Verosub, 1992). This was accomplished by normalizing individual major elements using the ratio of Zr in a sample to the ratio of Zr in the most relevant (least altered) rock sample. This normalization to Zr causes some difficulty for Bumpass Hell, where two precipitate samples have exceptionally high Zr (and thus appear more "leached" in the spider diagram). Zirconium is below detection for the precipitated Growler Hot Springs sinter deposits, which are therefore not plotted with the other sites.

Silica sinter vs. acid-sulfate silica enrichment. Different parts of the Lassen hydrothermal system exhibit both acid leaching or sinter deposition, which can both produce silica-rich deposits. In acid leached deposits, silica is residually enriched as other, more soluble cations are removed. These altered samples also typically contain elevated TiO_2 concentrations, because Ti is also less mobile under all but the most acidic conditions (e.g. Gray and Coolbaugh, 1994). Altered sediment samples L-LV-14-05 from Little Hot Springs Valley and L-BH-12-3 from Bumpass Hell are classic examples of this type of alteration, consisting of quartz ± anatase with elevated Si, Ti, and Zr concentrations (Figure 10A). In contrast, in near-neutral hot water environments, silica is precipitated from high temperature fluids, forming texturally discrete coatings on otherwise unrelated substrate rock. These deposits (as exemplified by sample L-13-G 3, which consists mostly of amorphous silica with clear evidence of biogenic precipitation: Figures 7 and 8) are characterized by high SiO_2 and low TiO_2 contents (Figure 10B), because Ti is not readily transported by these fluids due to its low solubility. The two isocon diagrams in Figure 10 compare these representative samples of acid-sulfate

leached (A) or silica sinter precipitated (B) material against less altered rocks collected at or near the site, to illustrate trends in major element depletion and enrichment for these two end members. We recognize that the locally available less altered rock may not reflect the composition of the rocks from which the hydrothermal fluids originated, however this comparison is still useful for distinguishing between the products of acid-sulfate leaching and sinter precipitation in situations (such as on Mars) when the original environment is unknown.

Implications

Mineralogical and geochemical comparison between Lassen and Martian hydrothermal alteration

Direct comparison between the Lassen hydrothermal area and the Columbia Hills on Mars is complicated by several factors, including a significant difference in substrate composition (dacite and andesite versus high-Fe basalt), the availability of water (abundant snow and rainfall at Lassen), and the availability of free oxygen in the atmosphere to help oxidize surface mineral deposits. While the atmospheric conditions on Mars at the time of formation of the Columbia Hills hydrothermal deposits are poorly constrained, conditions were likely much drier than those of Lassen today. These differences are likely to manifest as: 1) more abundant Al-sulfate phases and less abundant Fe-sulfate phases at Lassen compared to Mars based on bulk compositional differences, 2) better preservation potential for soluble phases on Mars compared to Lassen, because of less availability of surface water, and 3) a dominance of opal-A (rather than more crystalline silica phases) in Martian silica-rich deposits compared to

552 Lassen hydrothermal deposits, due to either pre-existing crystalline silica in the Lassen
553 volcanic rocks and soils, or to limited water availability and colder temperatures on Mars,
554 limiting diagenetic maturation (e.g. Ruff et al., 2011).
555
556 The quartz, tridymite, and cristobalite detected in some hydrothermally-altered Lassen
557 samples could relate to earlier episodes of high-temperature alteration or to the more
558 silica-rich composition of the host rocks (unlike at Gusev crater), though tridymite has
559 recently been identified in silica-rich mudstones investigated by the Mars Science Lab
560 Curiosity rover at Gale crater (Buckskin outcrop of the Murray Formation: Morris et al.,
561 2016). This Buckskin occurrence of abundant well-crystalline tridymite has been
562 interpreted as evidence for silicic volcanism because of the high temperatures typically
563 associated with tridymite formation on Earth, though a fumarolic origin for the original
564 silica enrichment (later heated to allow for tridymite formation) cannot be ruled out (see
565 Getahun et al., 1996, for a terrestrial example), and minor tridymite has been identified
566 associated with silica sinters in Iceland (Preston et al., 2008).
567
568 The higher concentrations of iron in Mars basalts (especially in the Columbia Hills: 13.2
569 – 21.3 wt. % Fe_2O_3T, McSween et al., 2006) compared to the Lassen dacites and
570 andesites likely contributes to the greater abundance of Fe-sulfate phases observed near
571 Home Plate. Lassen hydrothermal sulfates are instead dominated by Al-rich phases,
572 though minor Fe-sulfates are present. The high solubility of certain Fe-sulfates (e.g.
573 copiapite: Bigham and Nordstrom, 2000) could also affect their relative abundances on a
574 colder, drier Mars and a warmer, wetter Lassen. Mg-sulfate minerals are exceedingly rare

575 at Lassen, likely because of their high solubility (Spencer, 2000), the availability of
576 surface water to remove dissolved cations from the system, and the relatively low
577 concentrations of Mg in the unaltered dacitic and andesitic country rocks.
578
579 The presence of silica-rich hydrothermal deposits formed by both acid-sulfate leaching
580 (e.g. Sulphur Works and Bumpass Hell) and near-neutral silica sinter precipitation
581 (Growler Hot Spring) provides a useful test for competing hypotheses regarding the
582 formation of the silica-rich soils observed by the Spirit Rover (Squyres et al., 2008; Yen
583 et al., 2008; Ruff et al., 2011). At Lassen, the Growler Hot Springs silica sinter is
584 enriched in silica but significantly depleted in Ti and all other elements compared to the
585 rocks on which they precipitate, while those formed through acid-sulfate leaching in
586 fumarolic environments show enriched (or at least unchanged) Ti concentrations due to
587 residual enrichment of relatively immobile elements.
588
589 Ti concentrations in silica-rich soils and outcrops near Home Plate on Mars do not appear
590 to be significantly depleted compared to nearby igneous substrate rocks (Squyres et al.,
591 2008; Ruff et al., 2011), with the 90% SiO_2 Kenosha Comets light-toned soil sample
592 showing a 50% enrichment in TiO_2 compared to average basaltic soil (Yen et al., 2008).
593 TiO_2 is also enriched in Fuzzy Smith, a silica-rich float rock from Home Plate (Ming et
594 al., 2008). These examples would be consistent with the acid-sulfate leaching examples
595 from Lassen. However, some experimental studies have shown that Ti can precipitate (as
596 anatase) from neutral to alkaline solutions sufficiently concentrated in Cl (e.g. Nam et al.,

1998; Kim et al., 1999); thus, the moderate concentration of Ti alone is insufficient to exclude a sinter origin for the Home Plate silica-rich deposits.

If some or all the Home Plate silica-rich deposits did form under near-neutral silica sinter conditions, the Lassen hydrothermal system could serve as an analog for how these conditions can occur as part of the same hydrothermal system as nearby acid-sulfate fumaroles. Sulfate-rich deposits in the vicinity of Home Plate are more consistent with formation under acid-sulfate conditions (e.g. Squyres et al., 2007; Schmidt et al., 2008, 2009). While the specific sulfate minerals present in the sulfur-rich soils near Home Plate (e.g. Paso Robles soils) cannot be determined using the tools available to the Spirit rover, interpretation of Mössbauer, APXS, and PanCam data shows that Fe^{3+} and Mg^{2+} rich sulfates likely dominate, along with some possible Ca-sulfate phases (Yen et al., 2008). A hydrothermal system like that at Lassen could allow for both types of deposit to form simultaneously within the same system (though at different locations), without the need to invoke multiple hydrothermal events.

Acknowledgements

The authors would like to thank the National Park Service for permission to access and sample hydrothermal areas within Lassen Volcanic National Park, Michael Magnuson at Lassen park for helping with our permits, safety plan, and site selection, and landowner Peter H. Seward for permission to access and sample Growler and Morgan Hot Springs. We also thank Teri Gerard, who assisted with 2012 and 2013 fieldwork and early

laboratory analyses, Gabrielle Walters for field assistance in 2012, the Gartons for generously offering the use of their cabin as a base of operations during fieldwork, Weon Shik Han for the use of his Hydrolab Sonde, and Harris Byers for his help developing the XRF sulfur calibration. This paper was greatly improved after insightful and constructive feedback from Steven Ruff, Michael Clynne, and David John. This work was funded by grants from the National Space Grant College and Fellowship Program though the Wisconsin Space Grant Consortium.

References

Arroyo, F.A., Siering, P.L, Hampton, J.S., McCartney, A., Hurst, M.P., Wolfe, G.V., and Wilson, M.S. (2015). Isolation and characterization of novel iron-oxidizing autotrophic and mixotrophic bacteria from Boiling Springs Lake, an oligotrophic, acidic geothermal habitat. Geomicrobiology Journal, 32, 140-157.

Bibring, J.-P., Langevin, Y., Mustard, J.F., Poulet, F., Arvidson, R., Gendrin, A., Gondet, B., Mangold, N., Pinet, P., Forget, F., and the OMEGA team (2006) Global mineralogical and aqueous Mars history derived from OMEGA/Mars Express data. Science, 312, 400-404.

Bigham, J.M., and Nordstrom, D.K. (2000). Iron and aluminum hydroxysulfates from acid sulfate waters. In: Alpers, C.N. et al., Eds. Sulfate Minerals. Reviews in Mineralogy and Geochemistry, V. 40, Mineralogical Society of America, Washington, D.C. pp. 351-403.

Byers, H., McHenry, L.J., and Grundl, T.J. (2016) Forty-nine major and trace element concentrations measured in Soil Reference Materials NIST SRM 2586, 2587, 2709a, 2710a and 2711a using ICP-MS and Wavelength Dispersive-XRF. Geostandards and Geoanalytical Research, 40, 433-445.

Clynne, M.P., Muffler, L.J.P., Siems, D.F., Taggart, J.E. Jr., and Bruggman, P. (2008) Major and EDXRF trace element chemical analyses of volcanic rocks from Lassen Volcanic National Park and vicinity, California. U.S. Geological Survey Open-File Report 2008-1091.

Clynne, M.A., Janik, C.J., and Muffler, L.J.P. (2003) “Hot water” in Lassen Volcanic National Park- Fumaroles, steaming ground, and boiling mudpots. U.S. Geological Survey Fact Sheet 101-02.

Day, A.L., and Allen, E.T. (1925) The Volcanic Activity and Hot Springs of Lassen Peak. The Carnegie Institution of Washington, Washington, 190pp.

Geptner, A.R., Ivanovskaya, T.A., and Pokrovskaya, E.V. (2005). Hydrothermal fossilization of microorganisms at the Earth's surface in Iceland. Lithology and Mineral Resources, 40, 505-520.

Getahun, A., Reed, M.H., and Symonds, R. (1996) Mount St. Augustine volcano fumarole wall rock alteration: Mineralogy, zoning, composition and numerical models of its formation process. Journal of Volcanology and Geothermal Research, 712, 73–107.

Goorissen, H.P., Boschker, H.T., Stams, A.J., and Hansen, T.A. (2003). Isolation of thermophilic *Desulfotomaculum* strains with methanol and sulfite from solfataric mud pools, and characterization of *Desulfotomaculum solfataricum* sp. nov. International Journal of Systematic and Evolutionary Microbiology, 53, 1223-1229.

Graetsch, H. (1994). Structural characteristics of opaline and microcrystalline silica minerals. In: Hearney, P.J., Prewitt, C.T., Ginnes, G.V., Eds. Silica: Physical behavior, geochemistry, and materials applications. Reviews in Mineralogy V. 29. Mineralogical Society of America, Washington, D.C., 209-232.

Gray, J.E., and Coolbaugh, M.F. (1994). Geology and geochemistry of Summitville, Colorado; an epithermal acid sulfate deposit in a volcanic dome. Economic Geology, 89, 1906-1923.

Herdianita, N.R., Browne, P.R.L., Rodgers, K.A., and Campbell, K.A. (2000) Mineralogical and textural changes accompanying ageing of silica sinter. Mineralium Deposita, 35, 48–62.

687 Hynek, B.M., Beach, M., and Hoke, M.R.T. (2010) Updated global map of Martian
688 valley networks and implications for climate and hydrologic processes. Journal of
689 Geophysical Research, 115, E09008.
690
691 Ingebritsen, S.E., Bergfield, D., Clor, L.E., and Evans, W.C. (2016). The Lassen
692 hydrothermal system. American Mineralogist, 101, 343-353.
693
694 Janik, C.J., and McLaren, M.K. (2010) Seismicity and fluid geochemistry at Lassen
695 Volcanic National Park, California: Evidence for two circulation cells in the
696 hydrothermal system. Journal of Volcanology and Geothermal Research, 189, 257-277.
697
698 John, D.A., Rytuba, J.J., Breit, G.N., Clynne, M.A., and Muffler, L.J.P. (2005)
699 Hydrothermal alteration in Maidu Volcano: A shallow fossil acid-sulfate magmatic-
700 hydrothermal system in the Lassen Peak area, California in Rhoden, H.N., Steininger,
701 R.C., and Vikre, P.G., eds., Geological Society of Nevada Symposium 2005: Window to
702 the World, Reno, Nevada, May 2005, 295-313.
703
704 John, D.A., Breit, G.N., Lee, R.G., Dilles, J.H., Muffler, L.P., and Clynne, M.A. (2006)
705 Fossil magmatic-hydrothermal systems in Pleistocene Brokeoff Volcano, Lassen
706 Volcanic National Park, California. American Geophysical Union, Fall Meeting 2006,
707 abstract #V53A-1745.
708

John, D.A., Breit, G.N., Lee, R., Dilles, J.H., Calvert, A.T., Muffler, L.J.P., Clynne, M.A., and Rye, R.O. (2009) Pleistocene magmatic-hydrothermal systems in the Lassen region, northeastern California. Geological Society of America Abstracts with Programs, 41(7), 525.

Kim, S.-J., Park, S.-D., Jeong, Y.H., and Park, S. (1999) Homogeneous precipitation of TiO_2 ultrafine powders from aqueous $TiOCl_2$ solution. Journal of the American Ceramic Society, 82, 927-932.

Knoll, A.H., Carr, M., Clark, B., Des Marais, D.J., Farmer, J.D., Fischer, W.W., Grotzinger, J.P., McLennan, S.M., Malin, M., Schröder, C., Squyres, S., Tosca, N.J., and Wdowiak, T. (2005). An astrobiological perspective on Meridiani Planum, Earth and Planetary Science Letters, 240, 179 – 189.

Konhauser, K.O., Phoenix, V.R., Bottrell, S.H., Adams, D.G., and Head, I.M. (2001). Microbial–silica interactions in Icelandic hot spring sinter: possible analogues for some Precambrian siliceous stromatolites. Sedimentology, 48, 415-433.

Krebs, J.E., Vaishampayan, P., Probst, A.J., Tom, L.M., Marteinsson, V.T., Andersen, G.L., and Venkateswaran, K. (2014). Microbial Community Structures of Novel Icelandic Hot Spring Systems Revealed by PhyloChip G3 Analysis. Astrobiology, 14, 229-240.

Le Bas, M.J., Le Maitre, R.W., Streckeisen, A., Zanettin, B., and IUGS Subcommission on the Systematics of Igneous Rocks (1986) A chemical classification of volcanic rocks based on the total alkali–silica diagram. Journal of Petrology, 27, 745–750.

Lynne, B.Y., Campbell, K.A., Perry, R.S., Browne, P.R.L., and Moore, J.N. (2006). Acceleration of sinter diagenesis in an active fumarole, Taupo volcanic zone, New Zealand. Geology, 34, 749-752.

Lynne, B.Y, Campbell, K.A., James, B.J., Browne, P.R.L., and Moore, J. (2007) Tracking crystallinity in siliceous hot-spring deposits. American Journal of Science, 307, 612-641.

McHenry, L.J. (2009) Element mobility during zeolitic and argillic alteration of volcanic ash in a closed-basin lacustrine environment: Case study Olduvai Gorge, Tanzania. Chemical Geology, 265, 540-552.

McHenry, L.J., Chevrier, V., and Schröder, C. (2011) Jarosite in a Pleistocene East African saline-alkaline paleolacustrine deposit: Implications for Mars aqueous geochemistry. Journal of Geophysical Research, 116, E04002.

McSween, H.Y., Ruff, S.W., Morris, R.V., Bell, J.F.III, Herkenhoff, K., Gellert, R., Stockstill, K.R., Tornabene, L.L., Squyres, S.W., Crisp, J.A., Christensen, P.R.,

McCoy, T.J., Mittlefehldt, D.W., and Schmidt, M. (2006) Alkaline volcanic rocks from the Columbia Hills, Gusev crater, Mars. Journal of Geophysical Research, 101, E09S91.

Ming, D.W., Gellert, R., Morris, R.V., Arvidson, R.E., Brückner, J., Clark, B.C., Cohen, B.A., d'Uston, C., Economou, T., Fleischer, I., and others (2008) Geochemical properties of rocks and soils in Gusev Crater, Mars: Results of the Alpha Particle X-Ray Spectrometer from Cumberland Ridge to Home Plate. Journal of Geophysical Research, 113, E12S39.

Morris, R.V., Klingelhöfer, G., Schröder, C., Fleischer, I., Ming, D.W., Yen, A.S., Gellert, R., Arvidson, R.E., Rodionov, D.S., Crumpler, L.S., and others (2008) Iron mineralogy and aqueous alteration from Husband Hill through Home Plate at Gusev crater, Mars: Results from the Mössbauer instrument on the Spirit Mars Exploration Rover. Journal of Geophysical Research, 113, E12S42.

Morris, R.V., Vaniman, D.T., Blake, D.F., Gellert, R., Chipera, S.J., Rampe, E.B., Ming, D.W., Morrison, S.M., Downs, R.T., Treiman, A.H., and others (2016) Silicic volcanism on Mars evidenced by tridymite in high-SiO_2 sedimentary rock at Gale crater. Proceedings of the National Academy of Sciences, 113, 7071–7076.

Muffler, L.J.P., and Clynne, M.A. (2015) Geologic field-trip guide to Lassen Volcanic National Park and vicinity, California. USGS Scientific Investigations Report 2015-5067.

777 Muffler, L.J.P., Nehring, N.L., Truesdell, A.H., Janik, C.J., Clynne, M.A., and
778 Thompson, J.M. (1982) The Lassen Geothermal System. Proceedings of the Pacific
779 Geothermal Conference, 1982. University of Auckland, New Zealand, pp. 349–356.
780
781 Nam, H.-D., Lee, B.-H., Kim, S.-J., Jung, C.-H., Lee, J.-H., and Park, S. (1998)
782 Precipitation of ultrafine crystalline TiO_2 powders from aqueous $TiCl_4$ solution by
783 precipitation. Japanese Journal of Applied Physics, 37, 4603-4608.
784
785 Pallister, J.S., Thornber, C.R., Cashman, K.V., Clynne, M.A., Lowers, H.A., Mandeville,
786 C.W., Brownfield, I.K., and Meeker, G.P. (2008) Petrology of the 2004–2006 Mount St.
787 Helens lava dome- implications for magmatic plumbing and eruption triggering, chap. 30
788 *in* Sherrod, D.R., Scott, W.E., and Stauffer, P.H., eds. A volcano rekindled: the renewed
789 eruption of Mount St. Helens, 2004–2006: U.S. Geological Survey Professional Paper
790 1750, p. 647–702.
791
792 Phillips, R.J., Zuber, M.T., Solomon, S.C., Golombek, M.P., Jakosky, B.M., Banerdt,
793 W.B., Smith, D.E., Williams, R.M.E., Hynek, B.M., Aharonson, O., and Hauck, S.A.
794 (2001). Ancient geodynamics and global-scale hydrology of Mars. Science, 291, 2587-
795 2591.
796
797 Preston, L.J., Benedix, G.K., Genge, M.J., and Sephton, M.A. (2008). A multidisciplinary
798 study of silica sinter deposits with applications to silica identification and detection of
799 fossil life on Mars. Icarus, 198, 331–350.

Robbins, S.J.; Di Achille, G., and Hynek, B.M. (2011). The volcanic history of Mars: High-resolution crater-based studies of the calderas of twenty volcanoes. Icarus, 211, 1179-1203.

Rodgers, K.A., Cook, K.L., Browne, P.R.L., and Campbell, K.A. (2002). The mineralogy, texture and significance of silica derived from alteration by steam condensate in three New Zealand geothermal fields. Clay Minerals, 37, 299-322.

Rodgers, K.A.; Browne, P.R.L., Buddle, T.F., Cook, K.L., Greatrex, R.A., Hampton, W.A., Herdianita, N.R., Holland, G.R., Lynne, B.Y., Martin, R., Newton, Z., Pastars, D., Sannazarrob, K.L., and Teece, C.I.A. (2004) Silica phases in sinters and residues from geothermal fields of New Zealand. Earth Science Reviews, 66, 1-61.

Ruff, S.W., Farmer, J.D., Calvin, W.M., Herkenhoff, K.E., Johnson, J.R., Morris, R.V., Rice, M.S., Arvidson, R.E., Bell, J.F.III, Christensen, P.R., and Squyres, S.W. (2011) Characteristics, distribution, origin, and significance of opaline silica observed by the Spirit rover in Gusev crater, Mars. Journal of Geophysical Research, 116, E00F23.

Ruff, S.W., and Farmer, J.D. (2016). Silica deposits on Mars with features resembling hot spring biosignatures at El Tatio in Chile. Nature Communications, 7, 13554. doi: 10.1038/ncomms13554.

Schmidt, M.E., Ruff, S.W., McCoy, T.J., Farrand, W.H., Johnson, J.R., Gellert, R., Ming, D.W., Morris, R.V., Cabrol, N., Lewis, K.W., and Schroeder, C. (2008) Hydrothermal origin of halogens at Home Plate, Gusev Crater. Journal of Geophysical Research, 113, E06S12.

Schmidt, M.E., Farrand, W.H., Johnson, J.R., Schröder, C., Hurowitz, J.A., McCoy, T.J., Ruff, S.W., Arvidson, R.E., Des Marais, D.J., Lewis, K.W., Ming, D.W., Squyres, S.W., and de Souza, P.A.Jr. (2009) Spectral, mineralogical, and geochemical variations across Home Plate, Gusev Crater, Mars indicate high and low temperature alteration. Earth and Planetary Science Letters, 281, 258-266.

Schulze-Makuch, D., Dohm, J.M., Fan, C., Fairén, A.G., Rodriguez, J.A.P., Baker, V.R., and Fink, W. (2007). Exploration of hydrothermal targets on Mars. Icarus, 189, 308-324.

Siering, P., Clarke, J.M., and Wilson, M.S. (2006) Geochemical and biological diversity of acidic, hot springs in Lassen Volcanic National Park: Geomicrobiology, 23, 129-141.

Spencer, R.J. (2000). Sulfate minerals in evaporite deposits. In: Alpers, C.N. et al., Eds. Sulfate Minerals. Reviews in Mineralogy and Geochemistry, V. 40, Mineralogical Society of America, Washington, D.C. pp. 173-192.

844 Squyres, S.W., Aharonson, O., Clark, B.C., Cohen, B.A., Crumpler, L., de Souza, P.A.,
845 Farrand, W.H., Gellert, R., Grant, J., Grotzinger, J.P., and others (2007) Pyroclastic
846 activity at Home Plate in Gusev Crater, Mars. Science, 316, 738-742.
847
848 Squyres, S.W., Arvidson, R.E., Ruff, S., Gellert, R., Morris, R.V., Ming, D.W.,
849 Crumpler, L., Farmer, J.D., Des Marais, D.J., and Yen, A. (2008) Detection of silica-rich
850 deposits on Mars. Science, 320, 1063-1067.
851
852 Summa, L.L., and Verosub, K.L. (1992) Trace element mobility during early diagenesis
853 of volcanic ash: applications to stratigraphic correlation. Quaternary International, 13-14,
854 149-157.
855
856 Thompson, J.M. (1985) Chemistry of thermal and nonthermal springs in the vicinity of
857 Lassen Volcanic National Park. Journal of Volcanology Geothermal Research, 25, 81-
858 104.
859
860 Walter, M.R., and Des Marais, D.J. (1993). Preservation of biological information in
861 thermal spring deposits: developing a strategy for the search for fossil life on Mars.
862 Icarus 101: 129-143.
863
864 Wang, A., Bell J.F.III, Li, R., Johnson, J.R., Farrand, W.H., Cloutis, E.A., Arvidson,
865 R.E., Crumpler, L., Squyres, S.W., and McLennan, S.M. (2008) Light-toned salty soils

and coexisting Si-rich species discovered by the Mars Exploration Rover Spirit in Columbia Hills. Journal of Geophysical Research, 113, E12S40.

White, D.E., Muffler, L.J.P., and Truesdell, A.H. (1971) Vapor-dominated hydrothermal systems compared with hot-water systems. Economic Geology, 66, 75-97.

Yen, A.S., Morris, R.V., Clark, B.C., Gellert, R., Knudson, A.T., Squyres, S., Mittlefehldt, D.W., Ming, D.W., Arvidson, R., McCoy, T., and others (2008) Hydrothermal processes at Gusev Crater: An evaluation of Paso Robles class soils. Journal of Geophysical Research, 113, E06S10.

Tables

Table 1: Samples descriptions and locations

Table 2: Hydrolab results for in-situ water analysis

Table 3: XRD results: non-sulfate minerals

Table 4: XRD results: sulfate minerals

Table 5: XRF results: major elements

Table 6: XRF results: trace elements

Figure Captions

Figure 1. Map of the southwest corner of Lassen Volcanic National Park, with sample sites indicated by stars. Little Hot Springs Valley samples were collected between the

upper (U) and lower (L) sites indicated. Growler and Morgan Hot Springs are beyond the park boundary (indicated by the thin, green line) to the south.

Figure 2. Model for hydrothermal fluid circulation within the Lassen hydrothermal system. The geothermal waters of the Lassen system are largely of meteoric origin, heated at depth by interaction with hot rock or magma. Hot water rises towards the surface and boils, segregating into acid-sulfate steam that feeds the higher elevation fumaroles, and residual near-neutral hot water that emerges at lower elevation hot springs. Figure based on model portrayed by Clynne et al., 2003 and described by Janik and McLaren, 2010.

Figure 3. Photos showing representative collection sites, with sample positions indicated. **A**. Sulphur Works fumarole. Temperature decreases with increasing distance from the center, and the surficial precipitate changes from one dominated by elemental sulfur near the steam vent to alunogen further out. Sample L-SW-12-2 is from the outer rind of the large rock in the center (which measures ~50 cm in length). **B**. Bumpass Hell outflow stream. The dark color on the margins (and the thin film on the surface of the water) comes from sulfide minerals (pyrite and marcasite, sample L-BH-12- 5) precipitating out of the reduced fluids as they are exposed to the surface. **C**. Travertine deposit in upper Little Hot Springs Valley, with abundant calcite-coated plant remains (sample L-LV-14-29). **D**. Bubbling mud pots in Little Hot Springs Valley. **E**. Fumarole alteration in lower Little Hot Springs Valley (samples L-LV-14-21, 22, and 23). Dark grey color is associated with more reducing conditions and the presence of abundant sulfide minerals

(marcasite, in L-LV-14-23). **F**. Growler Hot Spring, with silica sinter, gypsum, and halite-coated rocks (samples L-13-G-02 and 03).

Figure 4. Representative XRD plots, with main identified peaks labeled. Minerals: A = alunogen, Al = alunite, Am = amorphous (position of "hump" consistent with opal-A), C = cristobalite, G = gypsum, H = halotrichite ($Fe^{2+}Al_2(SO_4)_4 \cdot 22H_2O$), Ha= halite, J = jarosite, K = kaolinite, Kl = kalinite ($KAl(SO_4)_2 \cdot 11H_2O$), M = marcasite, P = pickeringite ($MgAl_2(SO_4)_4 \cdot 22H_2O$), Pl = plagioclase (substrate), Py = pyrite, Q = quartz, S = sulfur, Sm = smectite, V = voltaite ($K_2Fe^{2+}{}_5Fe^{3+}{}_3Al(SO_4)_{12} \cdot 18H_2O$). **A**. L-SW-12-14 (Sulphur Works, white to yellow "popcorn-like" precipitate near fumarole). The sample is dominated by quartz and contains sulfates (jarosite and alunogen), clays (kaolinite and smectite), and a minor amount of plagioclase, likely residual from the substrate. **B.** L-12-BH-5 (dark "scum" on margins of hot stream pictured in Figure 3B). Pyrite and marcasite indicate dominantly reducing conditions, while the presence of minor alunite and alunogen reveals incipient oxidation (or mixing between different sources). Silica is present as both cristobalite and quartz. **C.** L-LV-14-16. This sample contains a variety of sulfate minerals; note that halotrichite (H) and pickeringite (P), which differ from each other primarily based on substitution of Fe and Mg, were not distinguishable by XRD and are thus both included as possibilities. **D.** L-13-G-2 (precipitate on rocks at Growler Hot Spring, pictured in Figure 3F). The pattern is dominated by an amorphous "hump," with moderate amounts of gypsum and halite.

933 Figure 5. Spider diagrams showing alteration trends for Little Hot Springs Valley, based
934 on major elements. Samples are normalized to Zr (the least variable element at Sulphur
935 Works), and then normalized against the relevant substrate sample. (**A**) LHSV "pit"
936 samples (variation with depth). Sample L-LV-14-05 is a Si, Ti, and Zr rich acid-sulfate
937 leached sample, with depletions in most other elements. (**B**) Lower LHSV spring-related
938 precipitates and rock coatings. Sample L-LV-14-18 is a red mud with high (35.6%) Fe_2O_3
939 and almost no diffraction peaks, likely consisting of amorphous Fe-bearing phases
940 (perhaps nanophase Fe oxides or hydroxides). Sample L-LV-14-14 is a coating that
941 contains both quartz and gypsum, resulting in elevated SiO_2 and CaO. **C**) Lower LHSV
942 outcrop samples (Figure 3E).
943
944 Figure 6: Spider diagrams showing alteration trends for Sulphur Works and Bumpass
945 Hell, based on major elements. Samples are normalized to Zr (the least variable element
946 at Sulphur Works), and then normalized against the relevant substrate sample. (**A**)
947 Sulphur Works, 2013 transect of sediment samples across a fumarole apron. (**B**) Sulphur
948 Works, altered rock and sediments samples within a fumarole apron (Figure 3A). Sample
949 L-SW-12-2 is the altered rim of a rock near the center of an active fumarole, the rest are
950 sediment and crust samples at varying distances from the vent. (**C**) Bumpass Hell. The
951 published composition of LC81-810 (an unaltered Bumpass Hell dacite, Clynne et al.,
952 2008) was used for normalization, as the least altered substrate sample we collected (L-
953 BH-12-8) still showed incipient alteration. Most elements are significantly depleted
954 compared to the substrate; in some cases (e.g. L-BH-12-3) this apparent depletion is
955 exaggerated because of anomalously high Zr concentrations.

Figure 7. Thin section photomicrographs for select samples, emphasizing the textures and context of silica-rich coatings. (**A**) Sample L-BH-12-2: plane-polarized light (PPL, above) and cross-polarized light (XPL, below) images. The field of view shows a subtle transition from the less altered interior (darker colored, left) to the more altered exterior (lighter colored, right) of an alteration rind. (**B**) Sample L-LV-14-14: PPL (above) and XPL (below). Shows the abrupt contact between a silica and gypsum-bearing precipitated crust (left) and the underlying andesitic host rock (right). (**C**) Sample L-13-G-2: PPL (above) and XPL (below). Shows abrupt contact between finely-laminated silica precipitate coating (sinter) and underlying andesitic substrate. (**D**) Sample L-13-G-2: PPL, 4x magnification (above) and 20x magnification (below). Textures show layering of the precipitated amorphous silica at the larger scale and the presence of biological materials at the finer scale.

Figure 8. Backscattered Electron (BSE) Scanning Electron Microscope (SEM) images of select thin sections. (**A** and **B**) BSE image of L-LV-14-14. Shows the abrupt contact between the underlying andesitic host rock (including plagioclase: Pl) and the overlying layered silica (Si) and gypsum (G)-rich precipitated crust. XRD data for this sample indicates only quartz as a silica-rich phase. (**C**) L-13-G-2. Finely laminated silica-rich precipitate overlying andesitic rock. Small, brighter grains within the sinter coating include pyroxene and potential dolomite. (**D** and **E**) L-13-G-3. Thin, hollow, silica-rich features within this sinter coating show evidence for biological activity. (**F**) L-BH-12-2.

978 The slightly altered rim of a Bumpass Hell rock sample, showing phenocrysts of
979 pyroxene and plagioclase with silica-rich phases in the groundmass.
980
981 Figure 9. **A**. Field photographs of the same fumarole at Sulphur Works taken in
982 September 2012, 2013, and 2014, with sample locations indicated. The coarse-grained,
983 fibrous alunogen sampled in 2012 was less abundant and finer grained in the following
984 years; these soluble sulfate precipitates are ephemeral and dependent on the presence of
985 surface water. **B.** XRD plots for the alunogen deposit, sampled in 2012 (L-SW-12-4),
986 2013 (L-13-SW-1), and 2014 (L-SW-14-03). In 2014, halotrichite and/or pickeringite (H)
987 was identified in addition to alunogen (A).
988
989 Figure 10. Isocon plots. **A.** Isocon plot for Bumpass Hell acid-sulfate altered sample (L-
990 BH-12-3) compared to the published composition of LC81-810 (a minimally altered
991 Bumpass Hell dacite, Clynne et al., 2008). Elements are scaled such that all can be
992 plotted within the same diagram (e.g., the wt. % of SiO_2 was divided by two for both the
993 altered sample and the substrate). The scaling factors used are indicated next to the name
994 of each oxide; all are in wt.% except for Zr which is in ppm. Elements plotting above the
995 1:1 line are enriched relative to the substrate, while elements below are depleted. In this
996 case, SiO_2, TiO_2, and Zr are all enriched, while most other elements are depleted. This is
997 consistent with acid-sulfate alteration, during which these immobile elements are
998 residually enriched while more mobile elements are leached from the system. **B.** Isocon
999 plot of Growler Hot Spring silica sinter (sample L-13-G-03) compared to andesitic rock
1000 sample L-LV-14-28. As expected for a precipitated silica sinter, only SiO_2 is enriched.

1001 The lack of Ti enrichment helps to distinguish precipitated from residual SiO_2-rich
1002 deposits.

This is a preprint, the final version is subject to change, of the American Mineralogist (MSA)
Cite as Authors (Year) Title. American Mineralogist, in press.
(DOI will not work until issue is live.) DOI: http://dx.doi.org/10.2138/am-2017-5839

This is a preprint, the final version is subject to change, of the American Mineralogist (MSA)
Cite as Authors (Year) Title. American Mineralogist, in press.
(DOI will not work until issue is live.) DOI: http://dx.doi.org/10.2138/am-2017-5839

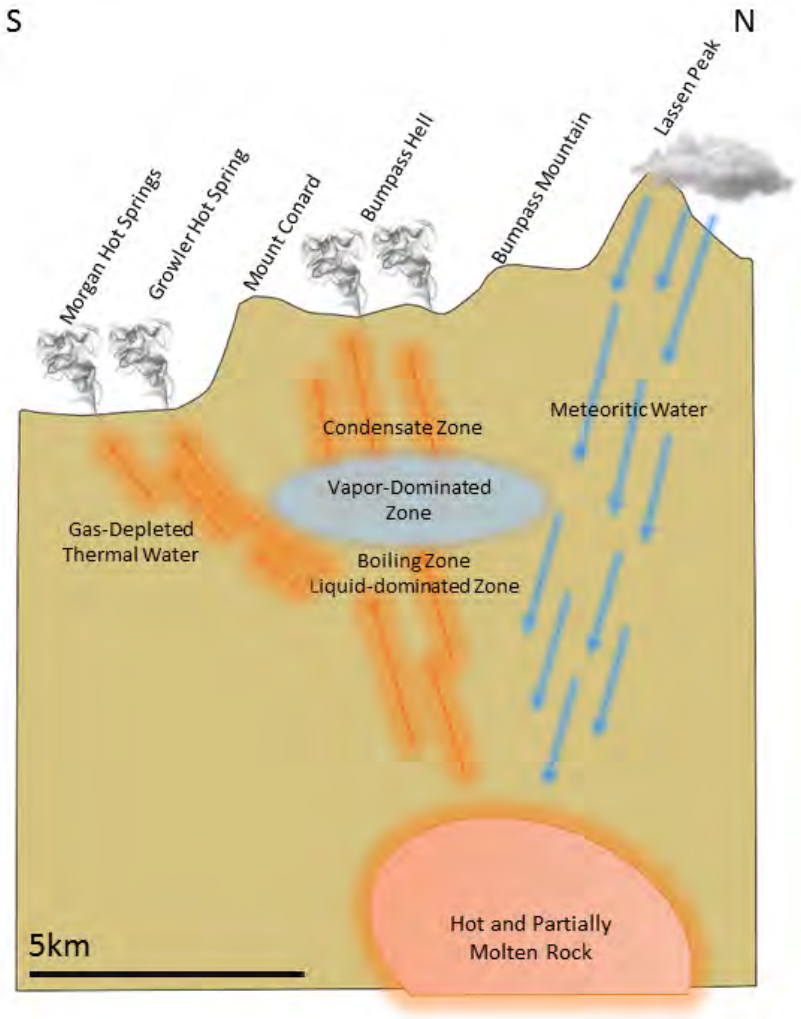

This is a preprint, the final version is subject to change, of the American Mineralogist (MSA)
Cite as Authors (Year) Title. American Mineralogist, in press.
(DOI will not work until issue is live.) DOI: http://dx.doi.org/10.2138/am-2017-5839

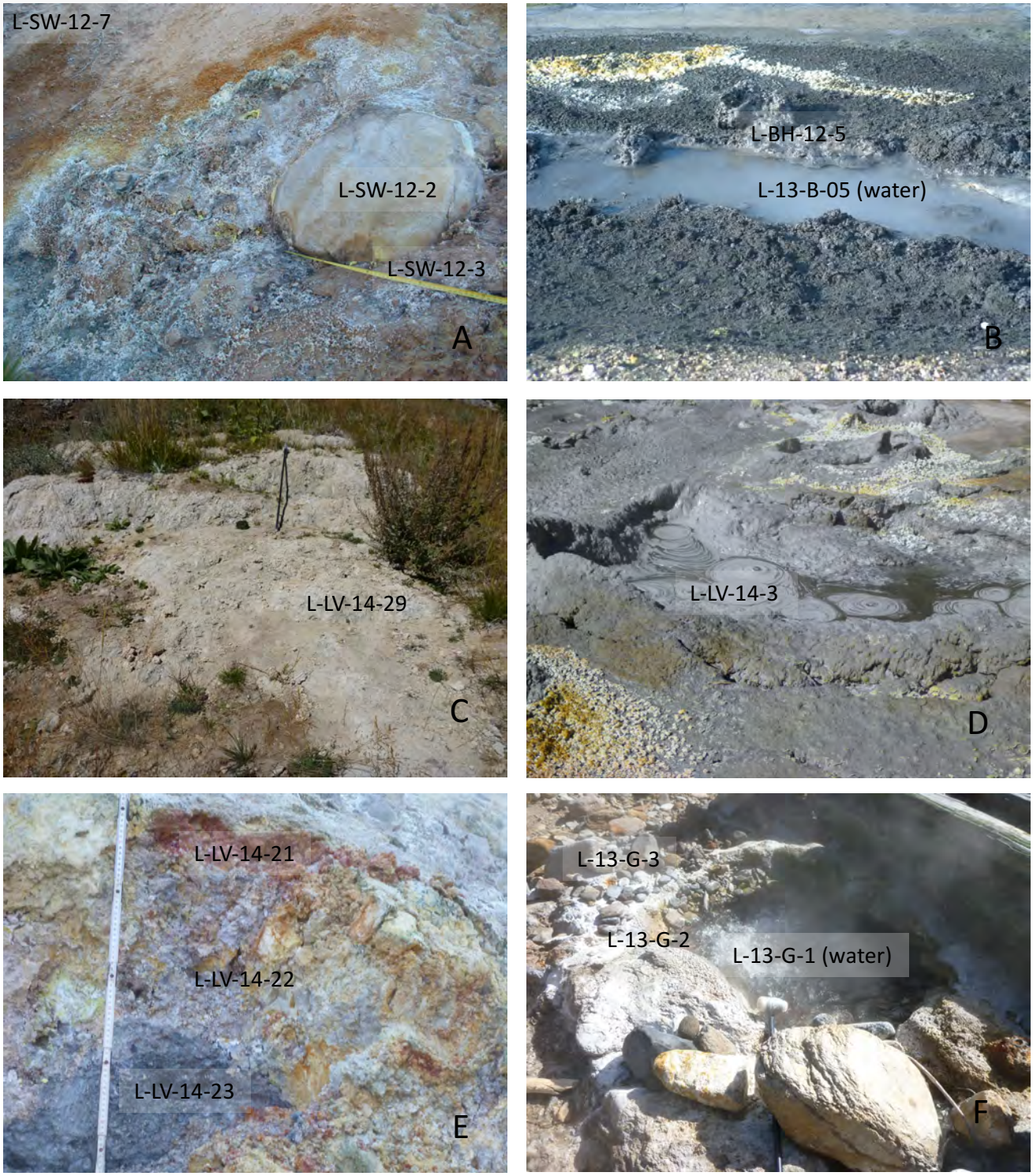

Figure 3

This is a preprint, the final version is subject to change, of the American Mineralogist (MSA)
Cite as Authors (Year) Title. American Mineralogist, in press.
(DOI will not work until issue is live.) DOI: http://dx.doi.org/10.2138/am-2017-5839

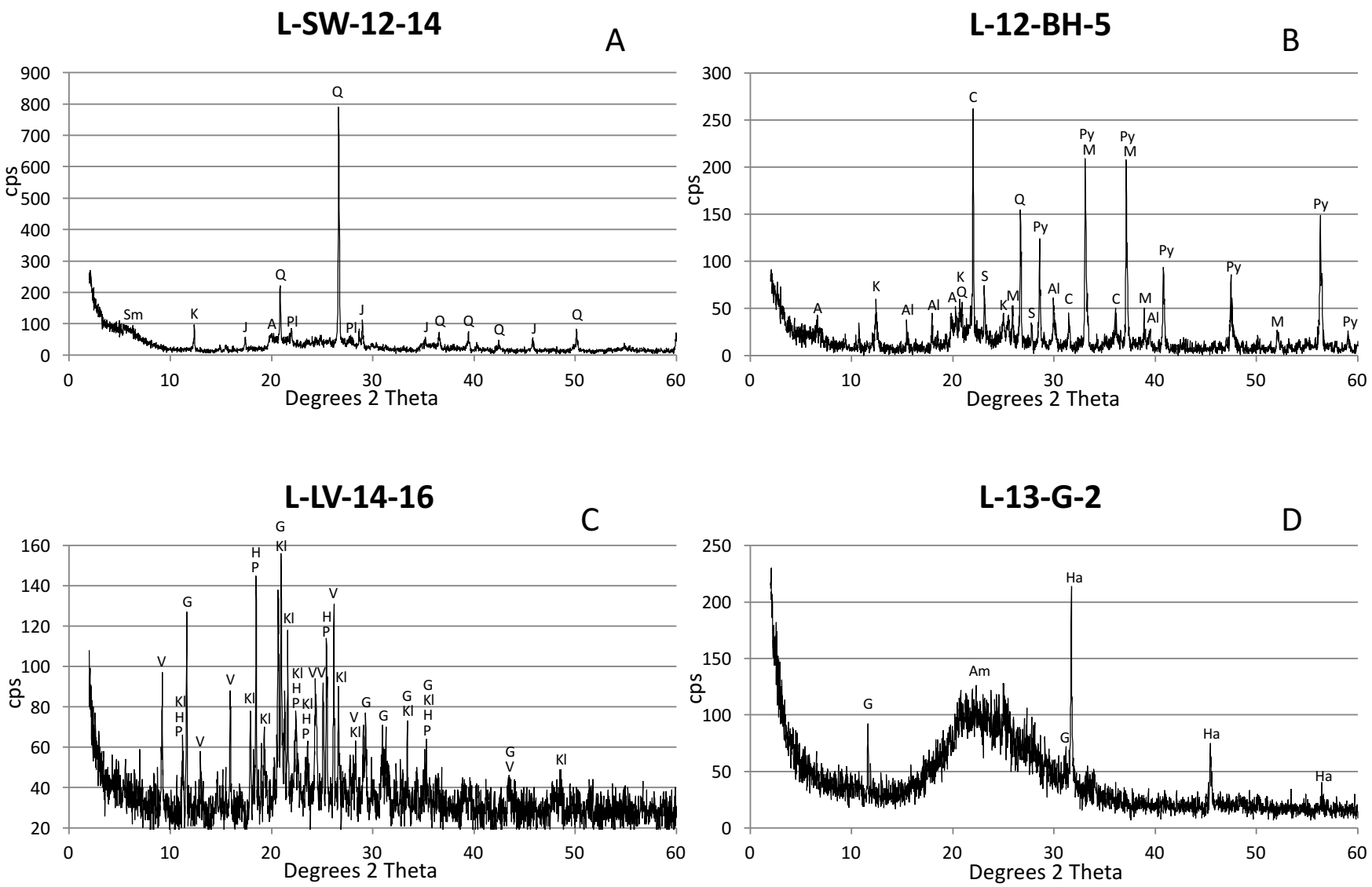

Figure 4

This is a preprint, the final version is subject to change, of the American Mineralogist (MSA)
Cite as Authors (Year) Title. American Mineralogist, in press.
(DOI will not work until issue is live.) DOI: http://dx.doi.org/10.2138/am-2017-5839

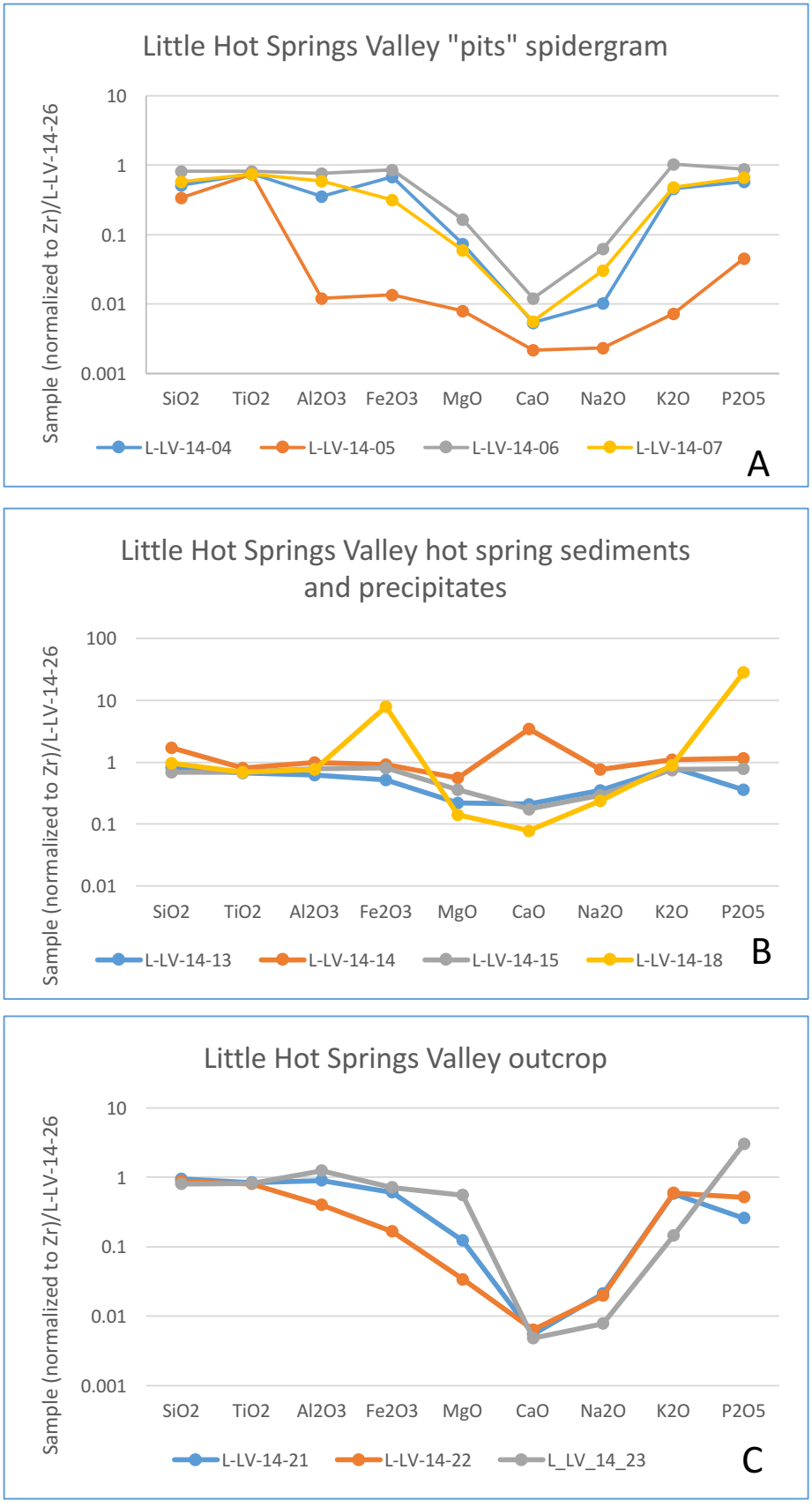

Figure 5

This is a preprint, the final version is subject to change, of the American Mineralogist (MSA)
Cite as Authors (Year) Title. American Mineralogist, in press.
(DOI will not work until issue is live.) DOI: http://dx.doi.org/10.2138/am-2017-5839

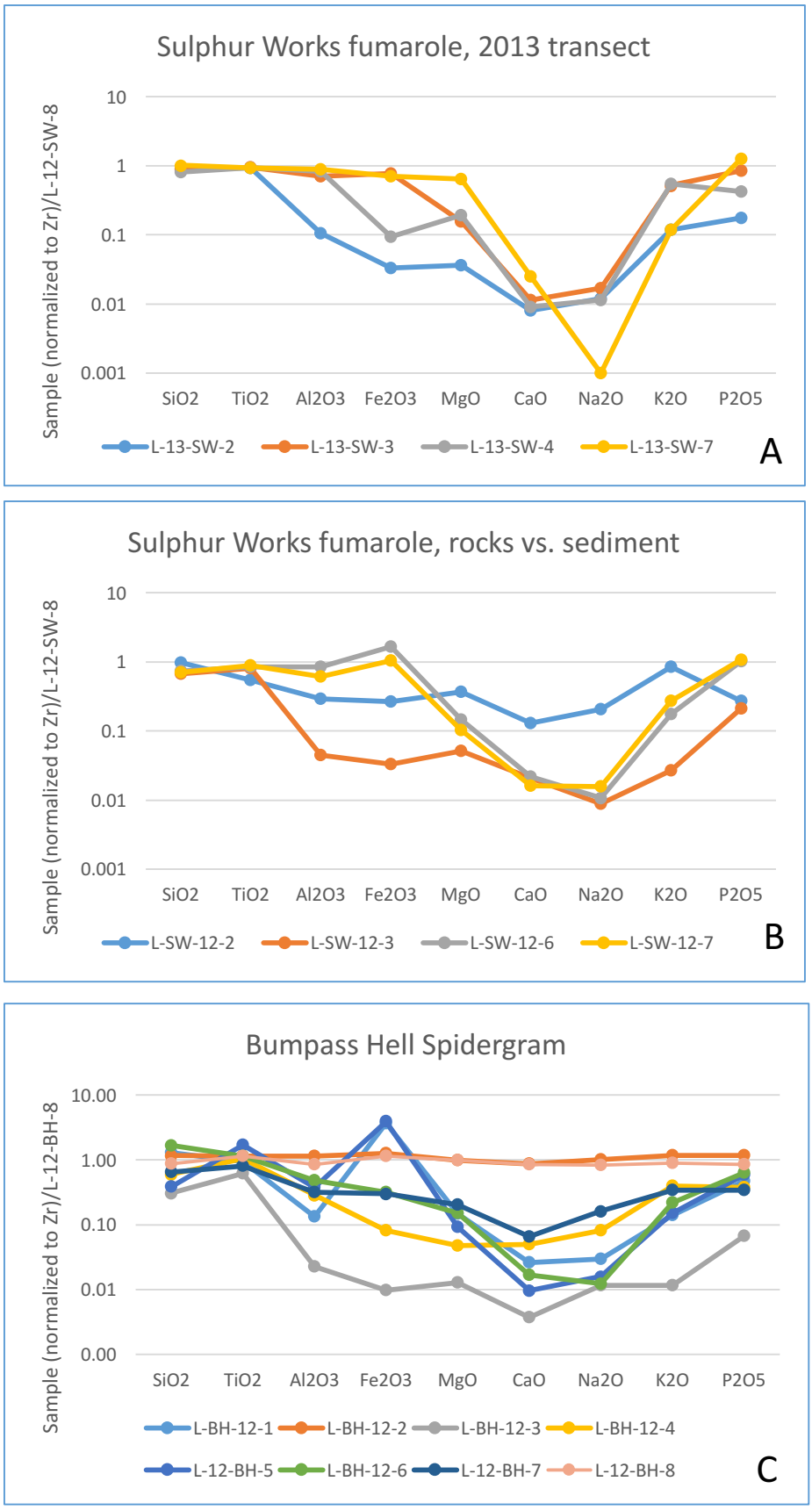

Figure 6

This is a preprint, the final version is subject to change, of the American Mineralogist (MSA)
Cite as Authors (Year) Title. American Mineralogist, in press.
(DOI will not work until issue is live.) DOI: http://dx.doi.org/10.2138/am-2017-5839

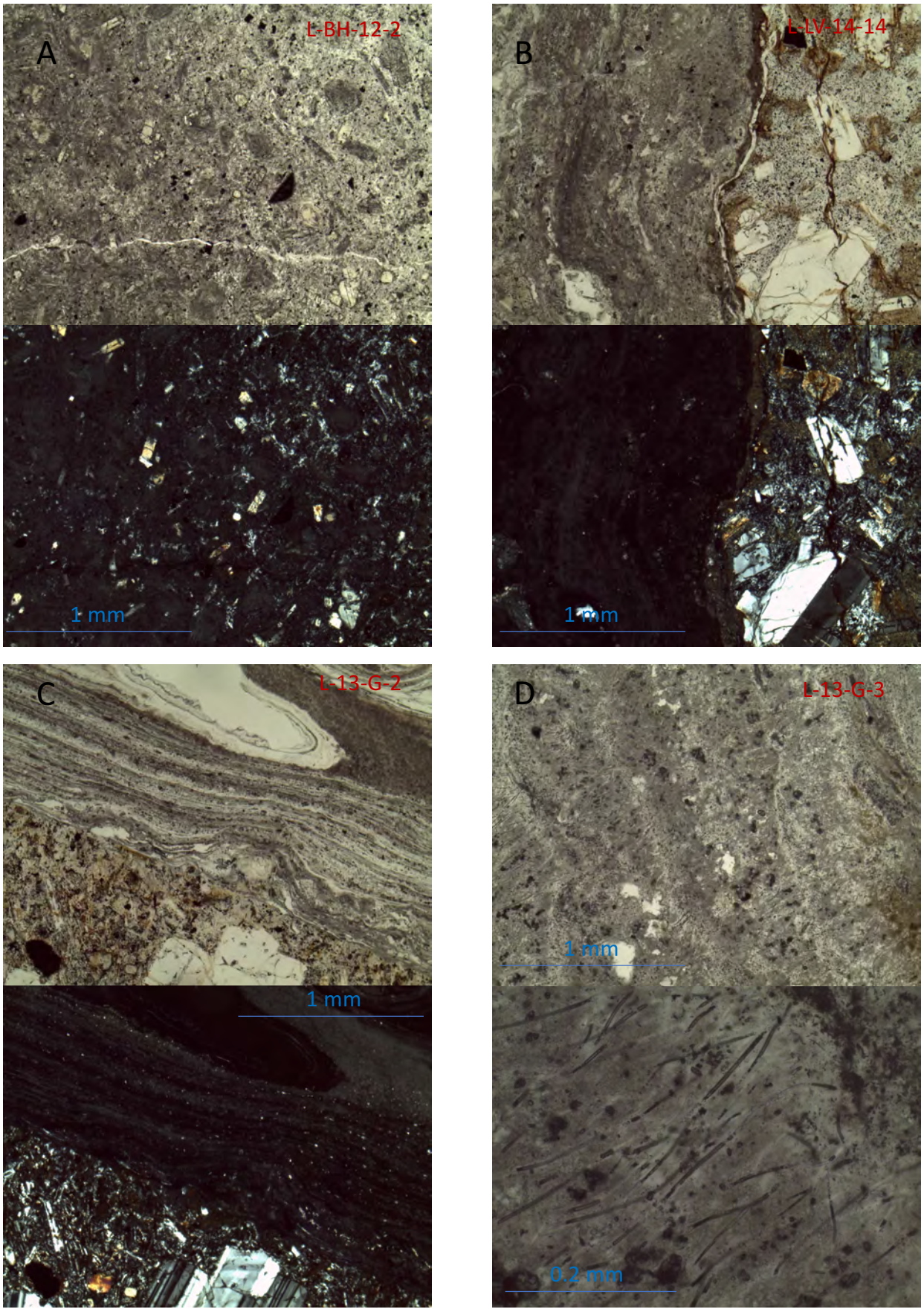

Figure 7

This is a preprint, the final version is subject to change, of the American Mineralogist (MSA)
Cite as Authors (Year) Title. American Mineralogist, in press.
(DOI will not work until issue is live.) DOI: http://dx.doi.org/10.2138/am-2017-5839

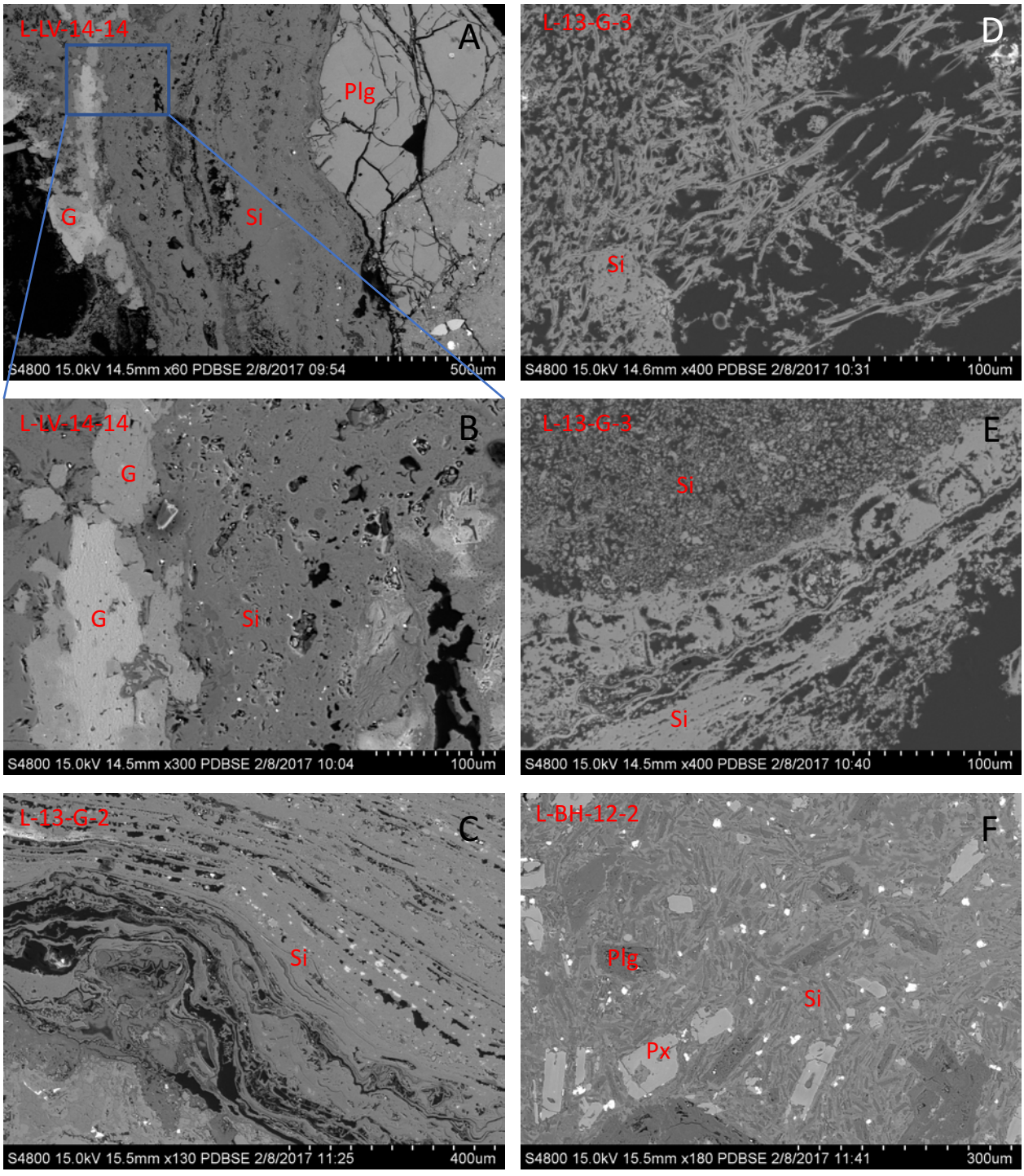

Figure 8

This is a preprint, the final version is subject to change, of the American Mineralogist (MSA)
Cite as Authors (Year) Title. American Mineralogist, in press.
(DOI will not work until issue is live.) DOI: http://dx.doi.org/10.2138/am-2017-5839

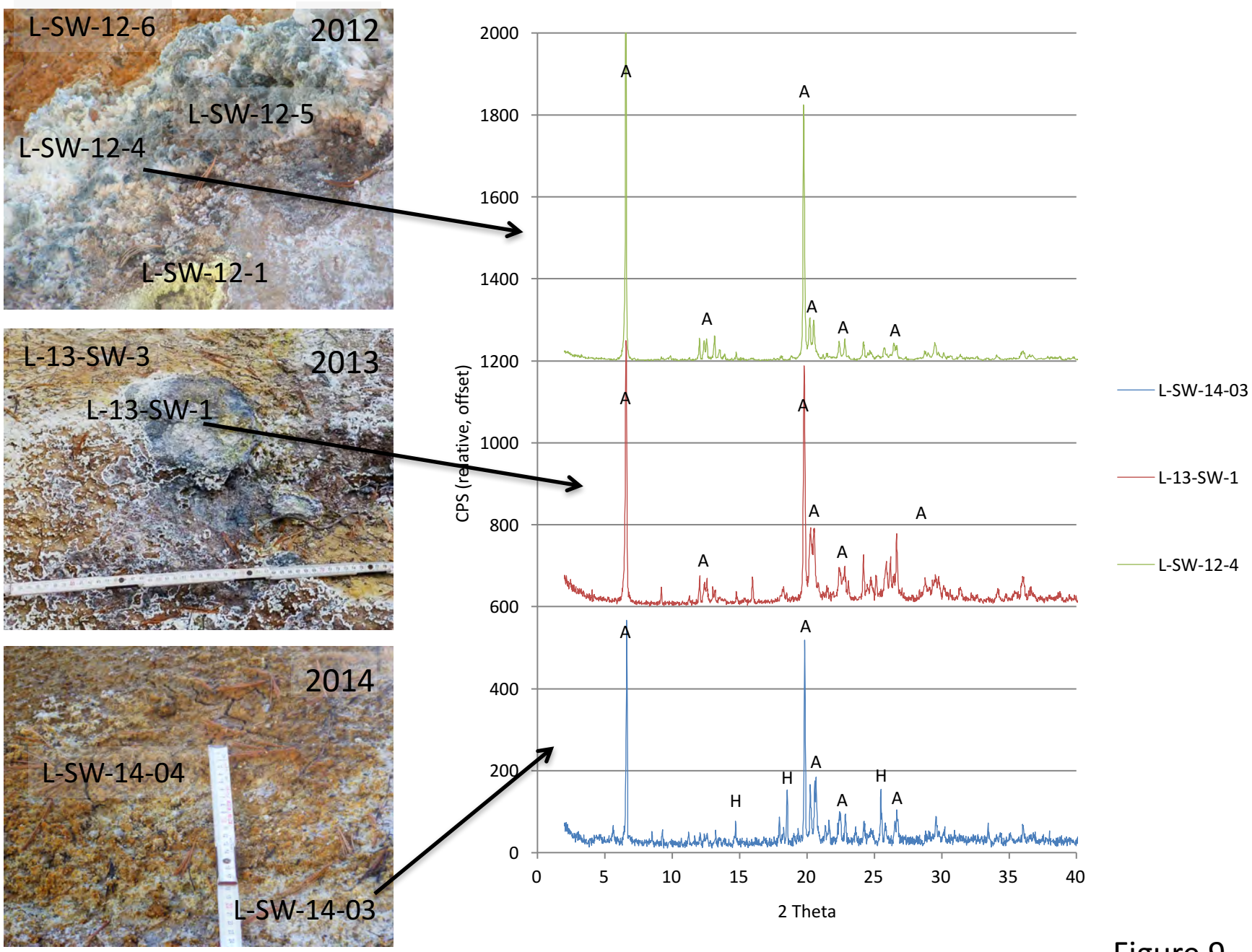

Figure 9

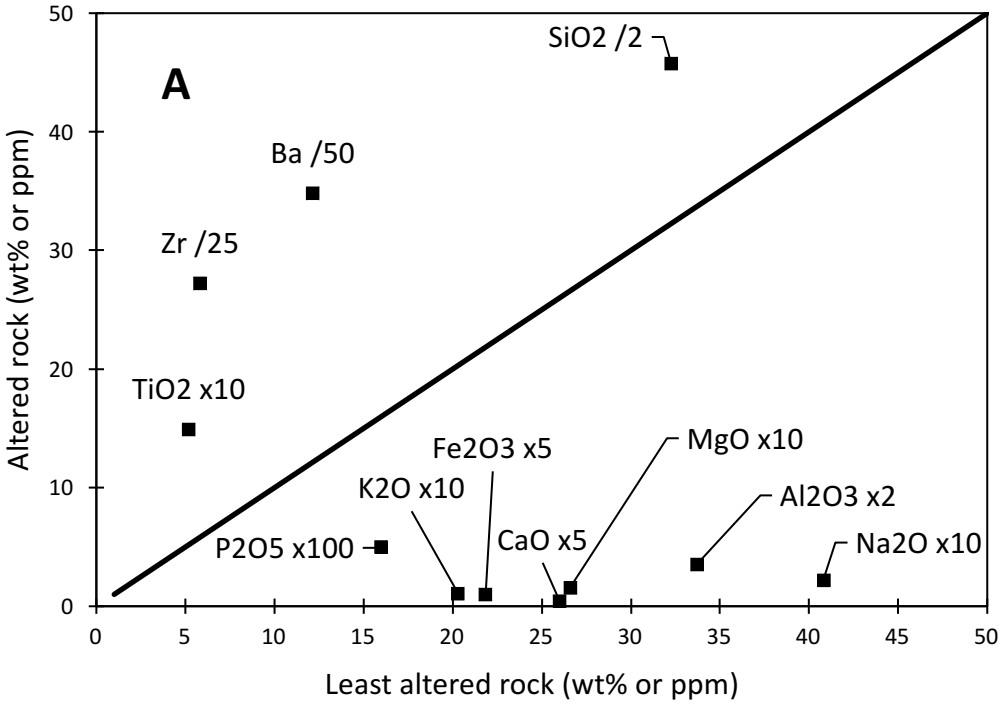

Bumpass Hell
Sample L-BH-12-3

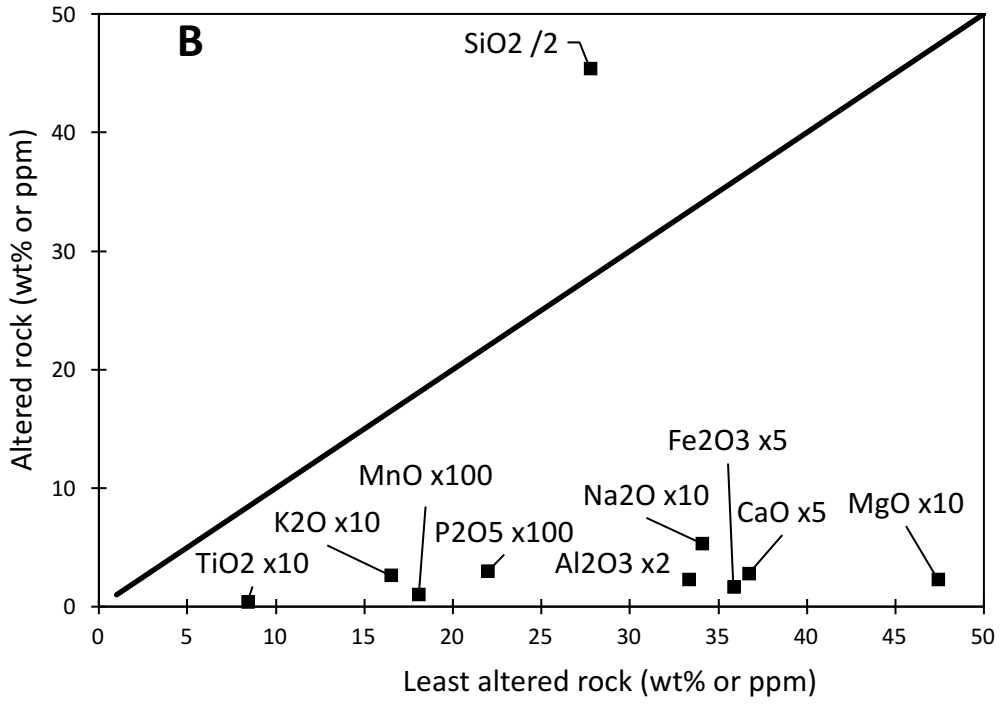

Growler Hot Spring
Sample L-13-G-3

Figure 10

This is a preprint, the final version is subject to change, of the American Mineralogist (MSA)
Cite as Authors (Year) Title. American Mineralogist, in press.
(DOI will not work until issue is live.) DOI: http://dx.doi.org/10.2138/am-2017-5839

Table 1: Sediment, precipitate, substrate, and rock sample descriptions and locations

Site	Name	Sample	Sample description	T (°C)	pH	GPS (WGS 84) N	W	Elev (m)
Sulphur Works								
	L-SW-12-1	precip	Yellow sulfur crystals, 1.7 m from center			40.45024	121.53542	2157
	L-SW-12-2	rock	Coating on rock near center of fumarole					
	L-SW-12-3	sed	Light brown crust, near rock at center					
	L-SW-12-4	precip	White, coarse, fibrous crystals, 1 m from center					
	L-SW-12-5	precip	Crystalline, yellow-orange, 0.7 m from center					
	L-SW-12-6	sed	Red-orange crust over grey sediment, 4.7 m from center					
	L-SW-12-7	sed	Light pink/grey crust, 5 m from center of fumarole					
	L-SW-12-10	precip	fibrous white, yellow, and red crystals, 1 m from mud pot	68.5	2.1			
	L-SW-12-11	precip	Orange and white crystals, next to stream from mud pot					
	L-SW-12-12	precip	White, orange, yellow, brown xtals, next to mud pot stream					
	L-SW-12-13	precip	Black, grey, white, red small xtals, next to mud pot stream					
	L-SW-12-14	precip	White, yellow popcorn-like xtals, on slope below mud pots					
	L-SW-12-15	sed	Grey muddy sediment, on slope below mud pots					
	L-SW-12-16	precip	White, fluffy crystals near bubbling mud pot					
	L-SW-12-17	precip	Yellow-white crystals on black substrate, near mud pot					
	L-SW-12-18	subst	Less altered substrate sample					
	L-13-SW-1	precip	White crystal coating, 1 m from vent	77.0				
	L-13-SW-2	sed	Beige, altered sediement surrounding vent	90.6				
	L-13-SW-3	sed	Orange, less crystalline material away from vent	25.9				
	L-13-SW-4	sed	Light grey sediment 3 cm below orange material	30.2				
	L-13-SW-7	sed	red/pink sediment	33.2		40.44927	121.53437	2126
	L-13-SW-8	subst	Minimaliy altered andesitic substrate sample					
	L-SW-14-2	precip	elemental sulfur/ tan sediment near steam vent	86.4	3.0	40.45025	121.53533	2154
	L-SW-14-3	precip	white crystals/ precipitate, 2 m from vent	66.6				
	L-SW-14-4	precip	orange crystals over off-white mud, 2 m from vent	46.6				
	L-SW-14-5	precip	white, crusty precipitate on rocks near vent	73.0				
	L-SW-16-05	subst	Darker substrate block upslope from altered area			40.45054	121.53434	2104
	L-SW-16-06	subst	Lighter, more weathered block upslope from altered area					
	L-SW-16-10	subst	Altered dacite upslope from modern altered area			40.44745	121.53407	2113
Bumpass Hell								
	L-BH-12-1	precip	Orange, yellow xtals over grey mud, near bubbling stream	81.0	2.5	40.45773	121.50183	2470
	L-BH-12-2	rock	Grey, altered rock near hot stream	65.0	2.4			
	L-BH-12-3	rock	Grey, altered rock w. few tiny, green crystal, from steaming pit					
	L-BH-12-4	precip	White, powdery minerals near edge of cool acid pool	17.5	3.0	40.45823	121.50078	2507
	L-BH-12-5	precip	Dark grey "foam" from edges of hot stream	27.1	2.2	40.45699	121.50052	2498
	L-BH-12-6	rock	Pink and white altered rock					
	L-BH-12-7	rock	Soft, powdery material over rotten dacite substrate			40.45747	121.50279	2506
	L-BH-12-8	subst	Slightly altered dacitic substrate			40.46394	121.50976	2512

pH of nearby thermal water, for samples adjacent to (or in contact with) hot springs, mud pots

Table 1, continued

Site	Name	Sample	Sample description	T (°C)	pH	GPS (WGS 84) N	W	Elev (m)
Little Hot Springs Valley								
	L-LV-14-2	sed	light grey/beige sediment from 40-cm pit 1	94.0	2.0	40.45586	121.51801	2170
	L-LV-14-3	sed	grey mud from mud pot					
	L-LV-14-4	sed	red/purple/orange sediment near surface of pit 2	44.0				
	L-LV-14-5	sed	white/cream sediment at 50 cm depth in pit 2	92.0		40.45564	121.51829	2173
	L-LV-14-6	sed	orange sediment near surface of pit 3	43.1				
	L-LV-14-7	sed	lavender mud at base of 37 cm pit 3	92.0				
	L-LV-14-9	precip	white precipitated crystals at surface	89.3		40.45603	121.51814	2181
	L-LV-14-10	sed	red mud in stream	35.8				
	L-LV-14-11	sed	yellow/orange mud, 23 cm deep in pit 4	31.2		40.45596	121.51825	2172
	L-LV-14-13	sed	Dark grey/black mud at bottom of pool	91.0		40.45290	121.51724	2121
	L-LV-14-14	precip	white precipitated crystal rock coating in stream					
	L-LV-14-15	rock	thick rock coating		1.7	40.45219	121.51673	2115
	L-LV-14-16	precip	thick, yellow crystalline rock coating	80.0				
	L-LV-14-17	precip	white, crinkly "ribbon" precipitate	71.0				
	L-LV-14-18	sed	Red mud from flowing hot spring	82.0	1.7			
	L-LV-14-20	coat	White, thick coating on rocks near bubbling hot spring	85.2	2.5			
	L-LV-14-21	sed	Red and orange, clayey sediment near top	47.6				
	L-LV-14-22	sed	light grey/purple with some yellow-orange clayey sediment	89.4				
	L-LV-14-23	sed	Dark grey, clayey sediment at base	92.6				
	L-LV-14-25	precip	off-white precipitate with many twigs, near hot spring			40.46143	121.52254	2284
	L-LV-14-26	subst	Minimally altered andesitic substrate					
	L-LV-14-27	precip	soft, white, flaky crust near hot spring	52.2	7.2			
	L-LV-14-28	rock	Altered substrate- red, orange, white, yellow					
	L-LV-14-29	precip	Formerly active travertine, white with many voids			40.46035	121.52097	2251
Growler (G) and Morgan (M) Hot Springs								
	L-13-G-2	precip	Sinter- white, hard coating on wet rocks near hot spring	93.5	8.1			
	L-13-G-3	precip	Sinter- white, hard coating on dry rocks near hot spring	93.5	8.1			
	L-13-M-1	precip	White and black dendritic material, 2 m from hot spring	49.6	7.0	40.38574	121.51468	1526
	L-13-M-2	precip	White, crusty crystals above pool, 0.9m from pool			40.38577	121.51467	1523
	L-13-M-3	precip	Orange, red tinted soft small crystals, edge of pool					
	L-13-M-4	precip	White and black dendritic material, 2 m from hot spring					
	L-13-M-6	precip	Crust from edge of pool, layered white, yellow-orange	49.3	7.0	40.38273	121.51419	1536

Table 2: Hydrolab results

		T (in situ) °C	T, °C* (HL)	pH (paper)	pH (HL)	ORP mV	SpCond uS/cm	Res kΩ-cm	Sal ppt	TDS g/l
Sulphur Works										
L-13-SW-5	hot spring	84.0	40.32		2.07	216	7206	0	4.01	4.6
L-13-SW-6	stream	8.8			6.71		267	4	0.13	0.3
L-SW-14-01	bubbling mud pot	82.0	16.13	2.3	3.24	-95	3069	0	1.66	2.0
Bumpass Hell										
L-13-B-01	Aqua cool pool	8.0			3.03	212	716	1	0.37	0.5
L-13-B-02	Hot acid pool	65.0	39.77		2.36	25	4334	0	2.37	2.8
L-13-B-03	cooler pool	19.7			2.15	-113	6012	0	3.32	3.8
L-13-B-04	warmer pool	40.2			2.02	-228	8005	0	4.48	5.1
L-13-B-05	pyrite stream	27.1			2.20	-190	4437	0	2.43	2.8
L-13-B-06	hottest pool	86.2	31.76		2.15	-175	5465	0	3.01	3.5
L-13-B-07	stream	88.6	32.95		2.39	-223	4342	0	2.37	2.8
Little Hot Springs Valley										
L-LV-14-01	bubbling hot spring	80.3	16.34	2.0	2.60	-99	5924	0	3.27	3.8
L-LV-14-08	bubbling mud pot	82.0	16.67	2.0	2.68	-160	6170	0	3.41	3.9
L-LV-14-12	bubbling hot spring	91.0	16.48	6.4	6.82	-314	409	2	0.20	0.3
L-LV-14-19	flowing hot spring	75.0	16.69	1.7	2.44	-153	9054	0	5.10	5.8
L-LV-14-24	hot spring	65.7	48.83	6.6	7.48	-488	1314	1	0.69	0.8
Growler/Morgan										
Growler	bubbling hot spring	93.5	37.82		8.09	-258	10963	0	6.23	7.0
Morgan	warm spring		49.26		7.01	-229	9459	0	5.34	6.1

* Only samples under 50°C can be analyzed in situ by hydrolab. T (in situ) = temperature at time of collection. T (HL) = temperature at the time of hydrolab analysis, if different.
ORP: Oxidation/reduction potential. SpCond: specific conductivity. Res: resistivity.
Sal: salinity. TDS: total dissolved solids. Ppt = parts per thousand.

Table 3: Non-sulfate phases identified by XRD

		Amorphous	Quartz	Cristobalite	Tridymite	Halite	Sulfur	Pyrite	Marcasite	Hematite	Anatase	Calcite	Kaolinite	Smectite	Substrate
Sulphur Works															
L-SW-12-1	precip	-	XXX	-	-	-	XXX	-	-	-	-	-	-	-	-
L-SW-12-2	rock	XXX	-	-	-	-		-	-	-	-	-	-	-	X
L-SW-12-3	sed	-	XXX	-	-	-	X	-	-	-	-	-	-	-	-
L-SW-12-4	precip	-	-	-	-	-		-	-	-	-	-	-	-	-
L-SW-12-5	precip	-	XXX	-	-	-	X	-	-	-	-	-	-	-	-
L-SW-12-6	sed	-	XXX	X	-	-	-	-	-	X	-	-	X	X	-
L-SW-12-7	sed	-	XXX	-	-	-	-	-	-	-	-	-	-	+	-
L-SW-12-10	precip	-	XXX	+	+	-	-	-	-	-	-	-	-	-	-
L-SW-12-11	precip	-	XXX	-	-	-	-	-	-	-	-	-	-	-	-
L-SW-12-12	precip	-	XXX	+	-	-	-	-	-	-	-	-	-	-	+
L-SW-12-13	precip	XX	XXX	XX	-	-	-	-	-	-	-	-	-	-	X
L-SW-12-14	precip	-	XXX	-	-	-	-	-	-	-	-	-	X	+	+
L-SW-12-15	sed	-	XXX	-	-	-	-	-	-	-	-	-	-	+	+
L-SW-12-16	precip	X	XX	-	-	-	-	-	-	-	-	-	-	-	-
L-SW-12-17	precip	XX	XXX	-	-	-	-	-	-	-	-	-	-	-	-
L-13-SW-1	precip	-	-	-	-	-	-	-	-	-	-	-	-	-	-
L-13-SW-2	sed	-	XXX	-	-	-	-	-	-	-	-	-	-	-	-
L-13-SW-3	sed	-	XXX	-	-	-	-	-	-	-	-	-	-	X	-
L-13-SW-4	sed	-	XXX	-	-	-	-	-	-	-	-	-	-	X	-
L-13-SW-7	sed	-	-	XX	-	-	-	-	-	-	-	-	-	-	XXX
L-13-SW-8	subst	-	-	-	-	-	-	-	-	-	-	-	-	-	XXX
L-SW-14-02	precip	-	XXX	-	-	-	XXX	-	-	-	-	-	-	-	-
L-SW-14-03	precip	-	-	-	-	-	-	-	-	-	-	-	-	-	-
L-SW-14-04	precip	-	XXX	-	-	-	-	-	-	-	-	-	-	XXX	-
L-SW-14-05	precip	-	XXX	-	-	-	-	-	-	-	-	-	-	+	-
L-16-SW-05	subst	-	-	-	-	-	-	-	-	-	-	-	-	X	XXX
L-16-SW-06	subst	-	+	-	-	-	-	-	-	-	-	-	-	X	XXX
L-16-SW-10	subst	-	+	-	-	-	-	-	-	-	-	-	-	-	XXX

XXX = abundant. XX = common. X= rare to common. + = rare
Precip: precipitate; sed: sediment; subst: less altered substrate.

Table 3, continued

		Amorphous	Quartz	Cristobalite	Tridymite	Halite	Sulfur	Pyrite	Marcasite	Hematite	Anatase	Calcite	Kaolinite	Smectite	Substrate
Bumpass Hell															
L-BH-12-1	precip	XX	-	-	-	-	XX	XX	+	-	-	-	-	-	-
L-BH-12-2	rock	-	XX	XX	XX	-	-	-	-	-	-	-	-	+	XX
L-BH-12-3	precip	XX	X	XXX	X	-	-	-	-	-	-	-	-	-	-
L-BH-12-4	precip	X	X	X	XXX	-	-	-	-	-	-	-	-	-	-
L-BH-12-5	precip	-	X	XX	-	-	X	XXX	X	-	-	-	X	-	-
L-BH-12-6	precip	-	XXX	-	-	-	-	-	-	-	-	-	+	+	-
L-BH-12-7	precip	X	+	XXX	+	-	-	-	-	-	-	-	-	-	+
L-BH-12-8	subst	-	-	XX	-	-	-	-	-	-	-	-	-	-	XXX
Little Hot Springs Valley															
L-LV-14-2	sed	-	XXX	-	-	-	-	-	-	-	-	-	-	+	-
L-LV-14-3	sed	-	XXX	-	-	-	-	-	-	-	-	-	XX	-	-
L-LV-14-4	sed	-	XXX	-	-	-	-	-	-	+	-	-	-	X	-
L-LV-14-5	sed	-	XXX	-	-	-	-	-	-	-	+	-	-	+	-
L-LV-14-6	sed	-	XXX	-	-	-	-	-	-	-	-	-	-	X	-
L-LV-14-7	sed	-	XXX	-	-	-	-	-	-	-	-	-	-	X	-
L-LV-14-9	precip	-	XX	-	-	-	-	-	-	-	-	-	-	-	-
L-LV-14-10	sed	-	XX	-	-	-	-	-	-	-	-	-	+	X	-
L-LV-14-11	sed	-	XXX	-	-	-	-	-	-	-	-	-	-	X	+
L-LV-14-13	sed	-	XXX	-	-	-	-	-	-	-	-	-	-	X	X
L-LV-14-14	precip	-	XX	-	-	-	-	-	-	-	-	-	-	X	X
L-LV-14-15	rock	-	XX	-	-	-	-	-	-	-	-	-	-	X	XX
L-LV-14-16	precip	X	-	-	-	-	-	-	-	-	-	-	-	-	-
L-LV-14-17	precip	-	X	-	-	-	-	-	-	-	-	-	-	-	-
L-LV-14-18	sed	+	-	-	-	-	-	-	-	-	-	-	-	-	-
L-LV-14-20	coat	X	-	-	-	-	XXX	-	-	-	-	-	-	-	X
L-LV-14-21	sed	+	XXX	-	-	-	-	-	-	-	-	-	-	XX	-
L-LV-14-22	sed	-	XXX	-	-	-	-	-	-	-	-	-	-	+	-
L-LV-14-23	sed	+	X	-	-	-	-	-	XX	-	-	-	+	XXX	-
L-LV-14-25	precip	-	-	-	-	-	-	-	-	-	-	XXX	-	+	-
L-LV-14-26	subst	-	-	-	-	-	-	-	-	-	-	-	-	+	XXX
L-LV-14-27	precip	-	-	-	-	-	-	-	-	-	-	XXX		+	-
L-LV-14-28	rock	-	XXX	-	-	-	-	-	-	-	-	-	-	-	-
L-LV-14-29	precip	-	+	-	-	-	-	-	-	-	-	XXX	-	+	-

Table 3, continued

		Amorphous	Quartz	Cristobalite	Tridymite	Halite	Sulfur	Pyrite	Marcasite	Hematite	Anatase	Calcite	Kaolinite	Smectite	Substrate
Growler (G) and Morgan (M) Hot Springs															
L-13-G-2	precip	XXX	-	-	-	XX	-	-	-	-	-	-	-	-	-
L-13-G-3	precip	XXX	-	-	-	-	-	-	-	-	-	-	-	-	-
L-13-M-1	precip	XXX	-	-	-	-	-	-	-	-	-	-	-	-	X
L-13-M-2	precip	XXX	-	-	-	-	-	-	-	-	-	-	-	-	X
L-13-M-3	precip	-	XXX	XX	-	-	-	-	-	-	-	-	-	-	X
L-13-M-4	precip	XXX	-	-	-	-	-	-	-	-	-	-	-	-	X
L-13-M-6	precip	XXX	X	-	-	XX	-	-	-	-	-	-	-	-	X

This is a preprint, the final version is subject to change, of the American Mineralogist (MSA)
Cite as Authors (Year) Title. American Mineralogist, in press.
(DOI will not work until issue is live.) DOI: http://dx.doi.org/10.2138/am-2017-5839

Table 4: Sulphate phases identified using XRD

		Alunite	Alunogen	Natroalunite	Kalinite	Tschermigite	Tamarugite	Voltaite	Jarosite	Lonecreekite	Quenstedtite	Rhomboclase	Halotrichite/ Pickeringite	Wroewolfeite	Gypsum
		$KAl_3(SO_4)_2(OH)_6$	$Al_2(SO_4)_3 \cdot 17H_2O$	$(Na,Ca_{0.5},K)Al_3(SO_4)_2(OH)_6$	$KAl(SO_4)_2 \cdot 11H_2O$	$(NH_4)Al(SO_4)_2 \cdot 12H_2O$	$NaAl(SO_4)_2 \cdot 6H_2O$	$K_2Fe^{2+}{}_5Fe^{3+}{}_3Al(SO_4)_{12}{\cdot}18H_2O$	$KFe^{3+}{}_3(SO_4)_2(OH)_6$	$(NH_4)Fe^{3+}(SO_4)_2 \cdot 12H_2O$	$Fe^{3+}{}_2(SO_4)_3 \cdot 11H_2O$	$(H_5O_2)Fe^{3+}(SO_4)_2 \cdot 2H_2O$	$(Mg,Fe^{2+})Al_2(SO_4)_4 \cdot 22H_2O$	$Cu_4(SO_4)(OH)_6 \bullet 2(H_2O)$	$CaSO_4 \cdot 2H_2O$
Sulphur Works															
L-SW-12-1	precip	-	-	-	-	-	-	-	-	-	-	-	-	-	-
L-SW-12-2	rock	-	-	-	-	-	-	-	-	-	-	-	-	-	-
L-SW-12-3	sed	-	-	-	-	-	-	-	-	-	-	-	-	-	-
L-SW-12-4	precip	-	XXX	-	-	-	-	-	-	-	-	-	-	-	-
L-SW-12-5	precip	-	-	-	-	-	-	-	-	-	-	-	-	-	-
L-SW-12-6	sed	-	X	-	-	-	-	-	-	-	-	-	-	-	-
L-SW-12-7	sed	-	-	-	-	-	-	-	+	-	-	-	-	-	-
L-SW-12-10	precip	-	-	-	-	-	-	-	-	-	-	-	-	-	-
L-SW-12-11	precip	-	-	-	-	-	-	-	-	-	-	-	-	-	-
L-SW-12-12	precip	-	+	-	-	-	-	-	-	X	-	-	-	-	-
L-SW-12-13	precip	-	X	-	-	-	+	-	-	-	-	-	-	-	-
L-SW-12-14	precip	-	+	-	-	-	-	-	X	-	-	-	-	-	-
L-SW-12-15	sed	-	-	-	-	-	-	-	-	-	-	-	-	-	-
L-SW-12-16	precip	-	X	-	-	XXX	-	-	-	-	-	-	-	-	-
L-SW-12-17	precip	-	+	-	-	XX	-	-	-	+	-	-	-	-	-
L-13-SW-1	precip	-	XXX	-	-	-	-	-	-	-	-	-	-	-	-
L-13-SW-2	sed	-	-	-	-	-	-	-	-	-	-	-	-	-	-
L-13-SW-3	sed	-	X	-	-	-	-	-	-	-	-	-	-	-	-
L-13-SW-4	sed	-	-	-	-	-	-	-	-	-	-	-	-	-	-
L-13-SW-7	sed	-	-	-	-	-	-	-	-	-	-	-	-	-	-
L-13-SW-8	subst	-	-	-	-	-	-	-	-	-	-	-	-	-	-

XXX = abundant. XX = common. X= rare to common. + = rare

Precip: precipitate; sed: sediment; subst: less altered substrate.

Table 4, continued

		Alunite	Alunogen	Natroalunite	Kalinite	Tschermigite	Tamarugite	Voltaite	Jarosite	Lonecreekite	Quenstedtite	Rhomboclase	Halotrichite/ Pickeringite	Wroewolfeite	Gypsum
Sulphur Works, continued															
L-SW-14-02	precip	-	-	-	-	-	-	-	-	-	-	-	-	-	-
L-SW-14-03	precip	-	XXX	-	-	-	-	-	-	-	-	-	XXX	-	-
L-SW-14-04	precip	-	X	-	-	-	-	-	-	-	-	-	-	-	-
L-SW-14-05	precip	-	-	-	-	-	-	-	-	-	-	-	-	-	-
L-16-SW-05	subst	-	-	-	-	-	-	-	-	-	-	-	-	-	-
L-16-SW-06	subst	-	-	-	-	-	-	-	-	-	-	-	-	-	-
L-16-SW-10	subst	-	-	-	-	-	-	-	-	-	-	-	-	-	-
Bumpass Hell															
L-BH-12-1	precip	-	-	-	-	-	-	-	-	-	-	X	-	-	-
L-BH-12-2	rock	-	-	-	-	-	-	-	-	-	-	-	-	-	-
L-BH-12-3	precip	-	-	-	-	-	-	-	-	-	-	-	-	-	-
L-BH-12-4	precip	-	-	X	-	-	-	-	-	-	-	-	-	-	-
L-BH-12-5	precip	X	+	-	-	-	-	-	-	-	-	X	-	-	-
L-BH-12-6	precip	-	-	-	-	-	-	-	-	-	-	-	-	-	-
L-BH-12-7	precip	-	-	-	-	-	-	-	-	-	-	-	-	-	-
L-12-BH-8	subst	-	-	-	-	-	-	-	-	-	-	-	-	-	-
		-	-	-	-	-	-	-	-	-	-	-	-	-	-
Little Hot Springs Valley		-	-	-	-	-	-	-	-	-	-	-	-	-	-
L-LV-14-2	sed	-	-	-	-	-	-	-	-	-	-	-	-	-	-
L-LV-14-3	sed	-	-	-	-	-	-	-	-	-	-	-	-	-	-
L-LV-14-4	sed	-	-	-	-	-	-	-	-	-	-	-	-	-	-
L-LV-14-5	sed	-	-	-	-	-	-	-	-	-	-	-	-	-	-
L-LV-14-6	sed	+	-	-	-	-	-	-	-	-	-	-	-	-	-
L-LV-14-7	sed	X	X	-	-	-	-	-	-	-	-	-	-	-	-
L-LV-14-9	precip	-	XX	-	-	-	-	-	-	-	-	-	XX	-	-
L-LV-14-10	sed	-	-	-	-	-	-	-	+	-	-	-	+	-	-
L-LV-14-11	sed	-	+	-	-	-	-	-	+	-	+	-	-	-	-
L-LV-14-13	sed	-	+	-	-	-	-	-	-	-	-	-	-	-	-
L-LV-14-14	precip	-	-	-	-	-	-	-	-	-	-	-	-	-	XXX
L-LV-14-15	rock	-	+	-	-	-	-	-	-	-	-	-	-	-	-
L-LV-14-16	precip	-	-	-	XX	-	-	XX	-	-	-	-	XX	-	XX
L-LV-14-17	precip	-	XXX	-	X	X	XX	-	-	-	-	-	XX	-	XX

This is a preprint, the final version is subject to change, of the American Mineralogist (MSA)
Cite as Authors (Year) Title. American Mineralogist, in press.
(DOI will not work until issue is live.) DOI: http://dx.doi.org/10.2138/am-2017-5839

Table 4, continued

		Alunite	Alunogen	Natroalunite	Kalinite	Tschermigite	Tamarugite	Voltaite	Jarosite	Lonecreekite	Quenstedtite	Rhomboclase	Halotrichite/ Pickeringite	Wroewolfeite	Gypsum
Little Hot Springs Valley, continued															
L-LV-14-18	sed	-	-	-	-	-	-	-	-	-	-	-	-	-	-
L-LV-14-20	coat	-	X	-	-	-	-	-	-	-	-	-	-	-	-
L-LV-14-21	sed	-	X	-	-	-	-	-	-	-	-	-	-	-	-
L-LV-14-22	sed	X	+	-	-	-	-	-	-	-	-	-	-	-	-
L-LV-14-23	sed	-	XX	-	-	-	-	-	-	-	-	-	-	-	-
L-LV-14-25	precip	-	-	-	-	-	-	-	-	-	-	-	-	-	-
L-LV-14-26	subst	-	-	-	-	-	-	-	-	-	-	-	-	-	-
L-LV-14-27	precip	-	-	-	-	-	-	-	-	-	-	-	-	-	-
L-LV-14-28	rock	-	-	-	-	-	-	-	-	-	-	-	-	X	-
L-LV-14-29	precip	-	-	-	-	-	-	-	-	-	-	-	-	-	-
Growler (G) and Morgan (M) Hot Springs															
L-13-G-2	precip	-	-	-	-	-	-	-	-	-	-	-	-	-	X
L-13-G-3	precip	-	-	-	-	-	-	-	-	-	-	-	-	-	-
L-13-M-1	precip	-	-	-	-	-	-	-	-	-	-	-	-	-	-
L-13-M-2	precip	-	-	-	-	-	-	-	-	-	-	-	-	-	X
L-13-M-3	precip	XXX	-	-	-	-	-	-	X	-	-	-	-	-	-
L-13-M-4	precip	-	-	-	-	-	-	-	-	-	-	-	-	-	-
L-13-M-6	precip	-	-	-	-	-	-	-	-	-	-	-	-	-	XX

Table 5: Bulk major element composition of Lassen hydrothermal altered samples, as measure by XRF, wt. % oxide

Site	Sample		SiO_2	TiO_2	Al_2O_3	Fe_2O_3	MnO	MgO	CaO	Na_2O	K_2O	P_2O_5	SO_3	LOI	Sum
Sulphur Works															
	L-SW-12-2	rock	78.67	0.65	6.50	2.36	0.05	2.07	1.08	1.02	2.21	0.09	NA	4.33	99.18
	L-SW-12-3	sed	61.63	1.10	1.15	0.34	ND	0.33	0.20	0.05	0.08	0.08	7.57	33.31	98.37
	L-SW-12-6	sed	56.55	0.95	17.72	13.98	0.01	0.77	0.17	0.05	0.43	0.32	9.14	8.28	99.43
	L-SW-12-7	sed	59.39	1.09	14.33	9.67	0.01	0.60	0.14	0.08	0.73	0.37	0.80	12.12	98.78
	L-SW-12-15	sed	86.72	0.83	5.35	1.49	0.01	0.50	0.51	0.49	0.91	0.11	NA	3.31	100.37
	L-SW-12-18	rock	76.31	0.68	9.14	0.10	ND	0.13	0.06	0.42	1.42	0.19	6.22	11.87	100.51
	L-13-SW-2	sed	88.07	1.32	2.80	0.35	ND	0.24	0.08	0.07	0.37	0.07	NA	5.75	99.29
	L-13-SW-3	sed	65.89	1.07	15.06	6.59	0.01	0.83	0.09	0.08	1.28	0.27	1.45	10.88	102.19
	L-13-SW-4	sed	68.74	1.18	19.58	0.89	0.01	1.14	0.08	0.06	1.51	0.15	NA	6.32	99.83
	L-13-SW-7	sed	66.17	0.91	16.11	5.14	0.01	2.93	0.17	ND	0.25	0.34	NA	7.48	99.67
	L-13-SW-8	sub	58.28	0.86	16.22	6.46	0.10	4.03	6.01	3.56	1.89	0.24	0.05	1.38	99.20
	L-SW-14-04	prec	57.81	1.01	16.94	7.11	ND	1.03	0.07	0.04	0.96	0.35	4.30	15.15	100.62
	L-SW-14-05	rock	95.19	0.69	1.78	0.09	ND	0.15	0.05	0.03	0.12	0.08	0.57	2.28	100.56
	L-SW-16-05	sub	55.36	1.16	16.25	7.57	0.07	3.62	6.85	3.48	1.69	0.42	NA	4.50	101.20
	L-SW-16-06	sub	55.39	1.07	15.20	6.47	0.07	2.62	5.55	2.79	1.72	0.39	NA	10.05	101.52
	L-SW-16-10	sub	61.92	0.80	16.16	5.26	0.05	2.05	2.96	2.68	1.92	0.19	NA	7.59	101.76
Bumpass Hell															
	L-BH-12-1	prec	55.25	0.32	1.51	10.67	ND	0.26	0.09	0.08	0.19	0.05	NA	28.76	97.29
	L-BH-12-2	rock	63.72	0.51	16.31	4.69	0.05	2.26	3.84	3.54	2.04	0.16	NA	2.17	99.45
	L-BH-12-3	prec	91.61	1.49	1.78	0.20	0.00	0.16	0.09	0.22	0.11	0.05	NA	5.35	101.31
	L-BH-12-4	prec	75.62	1.07	9.44	0.71	0.00	0.25	0.51	0.66	1.60	0.12	NA	10.5	100.62
	L-12-BH-5	prec	34.65	1.24	8.89	23.74	0.03	0.34	0.07	0.09	0.43	0.13	30.32	27.20	96.96
	L-BH-12-6	prec	85.70	0.47	6.47	1.10	ND	0.32	0.07	0.04	0.35	0.08	NA	2.99	97.68
	L-12-BH-7	prec	76.62	0.77	9.85	2.40	0.00	1.00	0.63	1.21	1.28	0.10	NA	6.12	100.21
	L-12-BH-8	sub	61.75	0.65	15.64	5.46	0.09	2.86	4.80	3.71	2.00	0.15	0.02	0.62	97.89
	LC81-810*	sub	64.52	0.52	16.86	4.37	0.08	2.66	5.20	4.08	2.03	0.16	NA	0.09	100.13
Little Hot Springs Valley															
	L-LV-14-04	sed	64.01	1.43	13.42	11.09	0.01	0.79	0.09	0.08	1.70	0.29	0.05	6.53	99.61
	L-LV-14-05	sed	93.98	3.13	1.02	0.49	ND	0.19	0.08	0.04	0.06	0.05	NA	0.82	100.10
	L-LV-14-06	sed	61.64	0.92	17.13	8.35	0.01	1.05	0.12	0.29	2.31	0.26	NA	7.95	100.19
	L-LV-14-07	sed	60.95	1.19	18.82	4.38	0.01	0.54	0.08	0.20	1.51	0.28	NA	11.50	99.67
	L-LV-14-13	sed	63.73	0.78	14.17	5.09	0.09	1.43	2.14	1.65	1.86	0.11	3.45	7.90	99.07
	L-LV-14-14	prec	48.28	0.34	8.26	3.35	0.04	1.33	12.77	1.31	0.92	0.13	0.82	11.92	88.79
	L-LV-14-15	rock	56.21	0.84	18.98	8.43	0.08	2.50	1.87	1.45	1.81	0.25	0.60	6.94	99.48
	L-LV-14-18	sed	33.00	0.36	7.94	35.63	0.01	0.42	0.36	0.50	0.91	3.83	2.57	16.08	99.15
	L-LV-14-21	sed	65.38	0.88	18.56	5.36	0.01	0.72	0.05	0.09	1.18	0.07	0.27	7.81	100.21
	L-LV-14-22	sed	72.57	1.00	9.88	1.78	ND	0.24	0.07	0.10	1.45	0.17	5.44	14.27	101.71
	L-LV-14-23	sed	49.72	0.77	23.41	5.77	0.05	2.95	0.04	0.03	0.27	0.75	4.17	17.47	101.33
	L-LV-14-26	sub	55.50	0.84	16.67	7.17	0.18	4.74	7.34	3.41	1.65	0.22	0.00	0.71	98.55
	L-LV-14-28	rock	70.23	0.79	15.12	5.09	ND	0.09	0.24	0.04	0.16	0.37	0.80	8.23	100.65
Growler and Morgan Hot Springs															
	L-13-G-2	prec	71.00	0.04	1.12	0.30	0.01	0.40	3.17	5.29	0.84	0.03	NA	9.16	91.36
	L-13-G-3	prec	90.80	0.04	1.14	0.33	0.01	0.23	0.55	0.53	0.26	0.03	0.05	6.38	100.31
	L-13-M-1	prec	81.56	0.27	3.98	1.74	0.03	0.70	1.45	1.67	0.85	0.05	NA	6.23	98.57
	L-13-M-2	prec	29.08	0.10	3.85	0.84	0.01	0.58	5.06	20.16	1.29	0.04	NA	38.14	99.19
	L-13-M-3	prec	52.79	1.00	11.11	8.76	0.01	0.91	0.36	0.44	2.15	0.30	NA	22.04	100.09

L-13-M-4	prec	82.18	0.27	4.47	1.96	0.01	0.74	1.34	1.32	0.78	0.06	NA	5.46	98.65
L-13-M-6	prec	66.12	0.29	5.55	2.15	0.03	0.87	3.25	4.16	1.02	0.07	3.32	13.45	97.02

Prec: precipitate, sed: sediment, sub: less-altered subtrate. All Fe reported as Fe_2O_3, all S reported as SO_3.

ND = not detected. NA = not analyzed.

* = data for Bumpass Hell dacite from Clynne et al., 2008.

Table 6: Bulk trace element composition of Lassen samples, as measured by XRF, ppm

Site	Sample		Zr	V	Zn	Ni	Cr	Ce	Sr	Ba
Sulphur Works										
	L-SW-12-2	rock	214	47	ND	ND	ND	186	96	1008
	L-SW-12-3	rock	245	ND	ND	ND	ND	184	128	312
	L-SW-12-6	sed	202	281	ND	ND	116	247	252	665
	L-SW-12-7	sed	222	264	ND	ND	106	252	207	1299
	L-SW-12-15	sed	168	55	ND	ND	44	170	109	470
	L-SW-12-18	rock	192	58	ND	ND	ND	99	452	888
	L-13-SW-2	sed	254	53	ND	ND	ND	190	68	1057
	L-13-SW-3	sed	203	228	ND	ND	84	199	99	597
	L-13-SW-4	sed	226	163	ND	ND	73	193	111	846
	L-13-SW-7	sed	173	155	43	ND	67	494	288	446
	L-13-SW-8	sub	154	154	65	74	105	208	442	579
	L-SW-14-04	prec	189	188	ND	ND	74	ND	142	584
	L-SW-14-05	rock	201	ND	ND	ND	ND	152	125	258
	L-SW-16-05	sub	157	196	75	72	163	73	744	729
	L-SW-16-06	sub	156	168	ND	74	160	74	652	656
	L-SW-16-10	sub	179	139	ND	30	96	87	411	855
Bumpass Hell										
	L-BH-12-1	prec	97	ND	ND	78	ND	217	65	427
	L-BH-12-2	rock	125	91	56	35	71	219	431	561
	L-BH-12-3	prec	680	ND	ND	ND	ND	ND	ND	1741
	L-BH-12-4	prec	289	70	ND	ND	43	118	198	549
	L-12-BH-5	prec	204	69	58	232	84	ND	231	499
	L-BH-12-6	prec	116	68	ND	ND	ND	101	170	418
	L-12-BH-7	prec	270	60	33	ND	45	ND	249	1291
	L-12-BH-8	sub	160	121	81	31	77	155	465	601
	LC81-810*	sub	146	NA	ND	ND	ND	NA	522	608
Little Hot Springs Valley										
	L-LV-14-04	sed	297	195	ND	ND	60	168	107	572
	L-LV-14-05	sed	662	ND	ND	ND	ND	ND	ND	1609
	L-LV-14-06	sed	178	277	ND	ND	87	ND	121	677
	L-LV-14-07	sed	252	138	ND	ND	69	144	503	897
	L-LV-14-13	sed	182	96	53	ND	56	ND	265	629
	L-LV-14-14	prec	67	53	36	ND	ND	120	894	445
	L-LV-14-15	rock	192	147	113	85	58	ND	217	479
	L-LV-14-18	sed	82	160	56	ND	ND	ND	202	360
	L-LV-14-21	sed	163	146	ND	ND	73	ND	ND	509
	L-LV-14-22	sed	196	60	ND	101	ND	ND	186	941
	L_LV_14_23	sed	148	183	ND	ND	86	143	82	297

L-LV-14-26	sub	132	193	69	42	98	144	430	551
L_LV_14_28	rock	140	145	ND	ND	74	ND	672	1702
Growler and Morgan Hot Springs									
L-13-G-2	prec	ND	ND	ND	ND	ND	ND	162	ND
L-13-G-3	prec	ND	ND	ND	ND	ND	ND	27	ND
L-13-M-1	prec	52	ND	ND	ND	ND	ND	175	189
L-13-M-2	prec	ND	ND	ND	ND	ND	150	259	47
L-13-M-3	prec	170	212	24	ND	128	147	839	492
L-13-M-4	prec	55	ND	ND	ND	ND	ND	158	214
L-13-M-6	prec	51	34	ND	ND	ND	165	274	183

Units = ppm. Prec= precipitate, sed= sediment, sub= less altered substrate.
ND = not detected.
* = data for Bumpass Hell dacite from Clynne et al., 2008.